

## ORIGINAL ARTICLE

# Nonparametric Measure-Transportation-Based Methods for Directional Data

Hallin M.<sup>1\*</sup> — Liu H.<sup>2†</sup> — Verdebout T.<sup>1‡</sup>

<sup>1</sup>ECARES and Département de Mathématique, Université libre de Bruxelles, Brussels, Belgium

<sup>2</sup>International Institute of Finance, School of Management, University of Science and Technology of China, Hefei, 230026, Anhui Province, P.R. China

## Correspondence

Marc Hallin, Université libre de Bruxelles, ECARES and Département de Mathématique, B-1050 Brussels, Belgium  
Email: mhallin@ulb.ac.be

## Funding information

\*Marc Hallin gratefully acknowledges the support of the COST (European Cooperation in Science and Technology) Action HiTEc CA21163 and the Czech Science Foundation grants GAČR22036365 and GA24-100788.

†Hang Liu's research is supported by the USTC grants WK2040000055 and YD2040002016.

‡Thomas Verdebout is supported by an ARC grant of the ULB and the Communauté Française de Belgique, a Projet de Recherche (PDR) grant of the FNRS, and the Fonds Thelam of the Fondation Roi Baudouin.

This paper proposes various nonparametric tools based on measure transportation for directional data. We use optimal transports to define new notions of distribution and quantile functions on the hypersphere, with meaningful quantile contours and regions and closed-form formulas under the classical assumption of rotational symmetry. The empirical versions of our distribution functions enjoy the expected Glivenko-Cantelli property of traditional distribution functions. They provide fully distribution-free concepts of ranks and signs and define data-driven systems of (curvilinear) parallels and (hyper)meridians. Based on this, we also construct a universally consistent test of uniformity and a class of fully distribution-free and universally consistent tests for directional MANOVA which, in simulations, outperform all their existing competitors. A real-data example involving the analysis of sunspots concludes the paper.

## KEYWORDS

directional statistics, directional quantiles, ranks, signs, optimal transport, directional GOF, directional MANOVA

## 1 — INTRODUCTION

Directional data analysis is dealing with random directions—taking values on circles and (hyper)spheres or, more generally, on manifolds. Directional data can be found in a variety of fields, including astronomy (Marinucci et al., 2008; Marinucci and Peccati, 2011), environmetrics (García-Portugués et al., 2014; Ameijeiras-Alonso et al., 2018; Kume and Sei, 2018), biology and medicine (Dryden, 2005; Hamelryck et al., 2006; Dortet-Bernadet and Wicker, 2008), to cite

only a few. Directions generally are represented as points on the unit hypersphere  $S^{d-1} := \{\mathbf{x} \in \mathbb{R}^d : \|\mathbf{x}\|^2 := \mathbf{x}^\top \mathbf{x} = 1\}$  in  $\mathbb{R}^d$ . The special nature of their sample spaces gives directional statistics a specific flavor. The models of interest are of the standard statistical types (one-sample and multi-sample location, analysis of variance, regression, etc.) and inference is carried out according to the usual principles, but their implementation takes special forms and requires distinctive techniques. A comprehensive exposition of the theoretical background and inference methods for circular and spherical data can be found in [Mardia and Jupp \(1999\)](#) or [Rao and SenGupta \(2001\)](#). More recent advances are presented in [Ley and Verdebout \(2017, 2018\)](#), while statistical tools for data on more general spaces are studied in [Chikuse \(2003\)](#) and [Bhattacharya and Bhattacharya \(2008, 2012\)](#).

The most popular parametric model in directional statistics, which can be traced back to the first decades of the 20th century, is the von Mises-Fisher model, characterized by the family of von Mises distributions, with densities (with respect to the classical surface area measure on  $S^{d-1}$ ) of the form

$$\mathbf{z} \in S^{d-1} \mapsto c_\kappa \exp(\kappa \mathbf{z}^\top \boldsymbol{\theta}), \quad (1.1)$$

where  $\boldsymbol{\theta} \in S^{d-1}$  plays the role of a location parameter,  $\kappa \in \mathbb{R}^+$ , which drives the probability mass in the vicinity of  $\boldsymbol{\theta}$ , is the so-called *concentration parameter*,  $c_\kappa$  is a normalizing constant, and  $\mathbf{z}^\top$  denotes the transpose of  $\mathbf{z}$ . The von Mises distribution is often seen as the “Gaussian directional distribution” due to the fact that the maximum likelihood estimator of  $\boldsymbol{\theta}$  is the normalized sample average.

The von Mises distributions belong to the more general class of rotationally symmetric distributions, which contains all distributions with densities (still with respect to the surface area measure on  $S^{d-1}$ ) of the form

$$\mathbf{z} \in S^{d-1} \mapsto c_f f(\mathbf{z}^\top \boldsymbol{\theta}), \quad (1.2)$$

where  $\boldsymbol{\theta} \in S^{d-1}$ ,  $f$  is some positive *angular function*, and  $c_f$  is a norming constant. The projection  $(I_p - \boldsymbol{\theta}\boldsymbol{\theta}^\top)\mathbf{Z}$  of a rotationally symmetric random vector  $\mathbf{Z}$  onto the tangent space (to  $S^{d-1}$ ) at  $\boldsymbol{\theta}$  has a spherical distribution. Inference for the parameters of rotationally symmetric distributions has been considered recently in [Christie \(2015\)](#), [Kanika et al. \(2015\)](#), and [Paindaveine and Verdebout \(2020a,b\)](#). Extensions of rotational symmetry yielding, after projection onto the tangent space (to  $S^{d-1}$ ) at  $\boldsymbol{\theta}$ , elliptically symmetric rather than spherical distributions have been proposed in [Kent \(1982\)](#), [Sealy and Wood \(2019\)](#), and [García-Portugués et al. \(2020\)](#); see also [Kume et al. \(2013\)](#), [Kume and Sei \(2018\)](#), and [Kent et al. \(2018\)](#).

Rank-based methods (including MANOVA) for directional data have been proposed in [Ley et al. \(2013, 2017\)](#) and [Verdebout \(2017\)](#). While the concepts of ranks considered there enjoy several attractive features, their distribution-freeness, hence also their applicability, is limited to the class of rotationally symmetric distributions. Based on sample projections onto the mean direction, the quantiles studied in [Ley et al. \(2014\)](#) are canonical for rotationally symmetric distributions on  $S^{d-1}$  but fail to be informative for general distributions on  $S^{d-1}$ .

The assumptions of rotational symmetry and their elliptical extensions are pervasive in the literature on directional data and can be compared, in this respect, to the assumptions of spherical and elliptical symmetry in traditional multivariate analysis. Just as the latter, they drastically simplify the mathematical structure of inference problems but also very severely restrict their validity: in most applications, rotational symmetry, indeed, is extremely unlikely to hold. The situation in the directional context, thus, is quite comparable to the situation in the general multivariate context: the absence of a canonical ordering, at first sight, precludes the canonical definition of essential order-related statistical tools as ranks, signs, and quantiles unless one is ready to make a very strong assumption of rotational symmetry (or its “elliptical extensions”) in the directional case, of spherical or elliptical symmetry in the general multivariate case. Based on measure transportation ideas and novel concepts of multivariate distribution and quantile functions in  $\mathbb{R}^d$ ,

new non- and semi-parametric methods have been proposed very recently in [Chernozhukov et al. \(2017\)](#) and [Hallin et al. \(2021a\)](#), which have demonstrated their efficiency in a variety of multivariate inference problems: see [Deb et al. \(2021\)](#), [Hallin et al. \(2021b\)](#), [Ghosal and Sen \(2022\)](#), [Hallin et al. \(2023, 2022a,b\)](#), [Shi et al. \(2022a,b\)](#), [del Barrio et al. \(2022\)](#), [Deb and Sen \(2023\)](#). [Torous et al. \(2022\)](#) use optimal transport to perform causal inference, while machine learning methods based on optimal transport have been proposed, e.g., in [Kolouri et al. \(2017\)](#). We refer to [Hallin \(2022\)](#) for a nontechnical survey.

The objective of this paper is to develop a measure-transportation-based approach for directional data similar to the one adopted in the above references, all of which are dealing with observations in  $\mathbb{R}^d$ . Measure transportation on hyperspheres and more general manifolds, however, is not a cosmetic adaptation of the Euclidean case, as it involves non-Euclidean topologies and metrics. As a consequence, the measure-transportation-based concepts and methods developed here do not follow along the same lines as in [Chernozhukov et al. \(2017\)](#) and [Hallin et al. \(2021a\)](#). Below, we mainly build upon [McCann \(2001\)](#), where the celebrated results of [McCann \(1995\)](#) on measure-preserving monotone mappings in  $\mathbb{R}^d$  are extended to Riemannian manifolds, to propose directional concepts of distribution and quantile functions inducing a distribution-specific system of curvilinear parallels and (hyper)meridians. These directional distribution functions can be seen as canonical transformations in the sense of [Jupp and Kume \(2020\)](#). The empirical counterparts of these concepts yield directional ranks, signs, and empirical quantiles enjoying the properties one is expecting from such notions (in particular, distribution-freeness of ranks and signs and quantile regions with prescribed probability contents irrespective of the underlying distribution); empirical distribution functions, moreover, are shown to satisfy a Glivenko-Cantelli consistency property.

The motivation for these definitions are the same as in  $\mathbb{R}$  and  $\mathbb{R}^d$ : conducting distribution-free inference based on ranks and signs, constructing quantile contours and (closed, connected, and nested) quantile regions, detecting directional outliers, defining directional values at risk, performing directional quantile regression, etc. Earlier attempts have been made with similar objectives, which are only partially successful: the notion of ranks studied in [Ley et al. \(2013, 2017\)](#) and [Verdebout \(2017\)](#), indeed, is not enjoying distribution-freeness unless the underlying distribution is rotationally symmetric; similarly, the quantile contours proposed in [Ley et al. \(2014\)](#) are satisfactory under rotational symmetry only.

In order to show that our measure-transportation-based concepts, contrary to earlier proposals, are achieving these objectives, we consider two very classical problems in directional inference:

- (i) (testing for directional uniformity) the classical problem of testing uniformity on  $S^{d-1}$ . This GOF problem is probably the oldest and most fundamental one in directional statistics, and can be traced back to the discussion by [Bernoulli \(1735\)](#) on whether the closeness of the orbital planes of various planets arose by chance or not. To cite only a few recent works, tests of uniformity in the context of noisy directional data were studied in [Lacour and Pham Ngoc \(2014\)](#) and [Kim et al. \(2016\)](#) and, in a high-dimensional context, in [Cai and Jiang \(2012\)](#), [Cai et al. \(2013\)](#), and [Cutting et al. \(2017\)](#). Projection-based tests were proposed by [Cuesta-Albertos et al. \(2009\)](#) and [García-Portugués et al. \(2023\)](#). Tests of uniformity were used in [García-Portugués et al. \(2020\)](#) in the problem of testing for rotational symmetry. Inference for location in the vicinity of uniformity was considered in [Paindaveine and Verdebout \(2017\)](#). We refer to [García-Portugués and Verdebout \(2018\)](#) for a recent review of this topic.
- (ii) (directional MANOVA) MANOVA on the hypersphere—testing the hypothesis of no-treatment effect, where the treatment can impact location, concentration, or skewness, is another very classical problem in directional inference. Due to the absence of distribution-free tools, the traditional approach typically reduces to a pseudo-von Mises MANOVA procedure—see for instance the recent contributions by [Figueiredo \(2006\)](#), [Ley et al. \(2017\)](#), [SenGupta and Kulkarni \(2020\)](#), and [Kulkarni and SenGupta \(2022\)](#), and the references therein; a major

weakness of pseudo-von Mises methods, however, is that their validity, which requires the classical Fisher consistency property, is guaranteed under rotational symmetry only.

In both cases, our directional measure-transportation-based concepts provide natural nonparametric and fully distribution-free solutions which (in simulations) perform equally well as some of their competitors under rotational symmetry and, most importantly, outperform them all in the non-rotationally-symmetric case:

- (i) (testing for directional uniformity) the directional distribution function for the uniform over  $S^{d-1}$  is the identity function; a (fully distribution-free) Cramér-von Mises-type test of uniformity on  $S^{d-1}$  based on our concept of empirical directional distribution function is shown to be *universally* consistent while outperforming (in simulations) its traditional competitors (the Rayleigh, Bingham, Ajne, Giné, and Bakshaev tests), as well as the more recent projection-based tests by [García-Portugués et al. \(2023\)](#). In sharp contrast with the universal consistency of our measure-transportation-based Cramér-von Mises test, these competitors, moreover, typically have undetectable *blind spots*. Also note that our measure-transportation-based Cramér-von Mises tests straightforwardly extend from testing uniformity to the general GOF problem;
- (ii) (directional MANOVA) the class of fully distribution-free MANOVA tests we are proposing is based on our concepts of directional ranks and signs; as in the traditional case of univariate rank tests, it involves the choice of a score function, which can target various types of alternatives. We provide the asymptotic ((non)central chi-square) distributions of the test statistics under the null and under local alternatives and show via simulations how our tests outperform their classical pseudo-von Mises competitors (the validity of which, moreover, is limited to the rotationally symmetric case).

The paper is organized as follows. In Section 2, we provide the relevant mathematical notions and briefly discuss the concept of measure transportation on Riemannian manifolds and hyperspheres. We define the population versions  $\mathbf{F}$  and  $\mathbf{Q}$  of our directional distribution and quantile functions in Section 3, then derive their explicit forms in the rotationally symmetric case. In Section 4, we introduce the empirical version  $\mathbf{F}^{(n)}$  of  $\mathbf{F}$  and establish its Glivenko-Cantelli asymptotic behavior by adapting the results of [Hallin et al. \(2021a\)](#) to the directional setup. Section 4.3 illustrates the construction of empirical quantile contours in simulated data. We also introduce new ranks and signs that are adapted to the directional setup. Our quantile contours, ranks and signs require a construction which is specific to the non-Euclidean context considered here (and therefore differs from the classical  $\mathbb{R}^d$  case). Under rotational symmetry, however, our quantile contours coincide with those of [Ley et al. \(2014\)](#), which are canonical for rotationally symmetric distributions; some distributional and equivariance properties of our signs and ranks are discussed in Supplementary Material A. In Section 5, we construct totally new Cramér-von Mises-type tests for goodness-of-fit based on  $\mathbf{F}^{(n)}$ , establish their universal consistency against fixed alternatives, and compare their performance with that of their many competitors. In Section 6, we propose a class of distribution-free MANOVA testing procedures and study their asymptotic distributions under the null and under local alternatives using the classical technical tools of [Hallin et al. \(2023, 2022a,b\)](#); we also establish their consistency under non-local alternatives. A real-data application is presented in Section 7, where we implement our MANOVA procedure on sunspots data. Finally, Supplementary Material A, B, C, and D are collecting (i) the basic properties of our ranks and signs, (ii) additional simulation results, (iii) an illustration of our quantile contours on a protein dataset, and (iv) the proofs of the various results provided in the paper.

## 2 — MEASURE TRANSPORTATION ON RIEMANNIAN MANIFOLDS

Throughout the paper, we denote by  $d(\mathbf{y}, \mathbf{z}) := |\arccos(\mathbf{y}^\top \mathbf{z})|$  the geodesic distance and by  $c(\mathbf{y}, \mathbf{z}) := d^2(\mathbf{y}, \mathbf{z})/2$  the squared Riemannian distance between two points  $\mathbf{y}$  and  $\mathbf{z}$  on the unit hypersphere  $S^{d-1}$ ; both  $c$  and  $d$  are continuous and bounded. When equipped with the geodesic distance,  $S^{d-1}$  is a separable complete metric space, hence a Polish metric space, with Borel  $\sigma$ -field  $\mathcal{B}^{d-1}$ . Denote by  $\lambda^{d-1}$  the *surface area measure* over  $S^{d-1}$ . Throughout, measurability tacitly is understood with respect to  $\mathcal{B}^{d-1}$  and  $P$  is assumed to be in the family  $\mathfrak{P}_d$  of  $\lambda^{d-1}$ -absolutely continuous distributions with densities bounded away from zero and infinity.

Measure transportation on Polish spaces and, more particularly, on Riemannian manifolds, is a well-studied subject; below, we mainly follow [McCann \(2001\)](#), where the celebrated results of [McCann \(1995\)](#) on measure-preserving monotone mappings in  $\mathbb{R}^d$  are extended to Riemannian manifolds, [Ambrosio and Pratelli \(2003\)](#), and [Schachermayer and Teichmann \(2008\)](#). Let  $P$  and  $Q$  denote two probability measures on  $S^{d-1}$ . Monge's optimal transport problem on  $S^{d-1}$  consists in minimizing, among the set  $S(P, Q)$  of all measurable transport maps  $S: S^{d-1} \rightarrow S^{d-1}$  such that  $(S\#P)(V) := P(S^{-1}(V)) = Q(V)$  for all  $V \in \mathcal{B}^{d-1}$  (in the measure transportation notation and terminology,  $S \in S(P, Q)$  is *pushing P forward to Q*), the transportation cost

$$C_M(S) := \int_{S^{d-1}} c(\mathbf{z}, S(\mathbf{z})) dP(\mathbf{z}) = \mathbb{E}_P[c(\mathbf{Z}, S(\mathbf{Z}))]. \quad (2.1)$$

Due to the fact that  $S(P, Q)$  is not convex, Monge's problem is an uneasy one.

Closely related to Monge's problem is the so-called Kantorovich problem. Denote by  $\Gamma(P, Q)$  the set of all probability measures  $\gamma$  on  $S^{d-1} \times S^{d-1}$  with "marginals"  $P$  and  $Q$ ; an element  $\gamma$  of  $\Gamma(P, Q)$  is called a *transport plan*. The Kantorovich problem on  $S^{d-1}$  consists in minimizing, among all transport plans  $\gamma \in \Gamma(P, Q)$ , the expectation

$$C_K(\gamma) := \int_{S^{d-1} \times S^{d-1}} c(\mathbf{y}, \mathbf{z}) d\gamma(\mathbf{y}, \mathbf{z}) \quad (2.2)$$

of the transportation cost  $c(\mathbf{Y}, \mathbf{Z})$  under  $(\mathbf{Y}, \mathbf{Z}) \sim \gamma$ . Unlike  $S(P, Q)$ , the set  $\Gamma(P, Q)$  is a convex subset of a Banach space; since  $c$  is bounded, the existence of a solution is guaranteed.

The Kantorovich problem is a relaxation of Monge's. Letting  $(I_d \times S)\mathbf{Z} := (\mathbf{Z}, S(\mathbf{Z}))$ , a transport map  $S \in S(P, Q)$  indeed induces a transport plan  $\gamma = (I_d \times S)\#P \in \Gamma(P, Q)$  which is concentrated on the graph of  $S$  (i.e., such that  $\gamma(\{(\mathbf{Z}, S(\mathbf{Z})) : \mathbf{z} \in S^{d-1}\}) = 1$ ) and satisfying  $C_K(\gamma) = C_M(S)$ . As we shall see ([Proposition 1](#) below), the solution of Kantorovich's problem is precisely of the form  $(I_d \times F)\#P$  where  $F$ , thus, is a solution of Monge's problem, and

$$C_M(F) = \min_{S \in S(P, Q)} C_M(S) = \min_{\gamma \in \Gamma(P, Q)} C_K(\gamma) = C_K((I_d \times F)\#P),$$

where  $\min_{\gamma \in \Gamma(P, Q)} C_K^{1/2}(\gamma) := \mathcal{W}_2(P, Q)$  is the Wasserstein distance between  $P$  and  $Q$ .

Before providing more precise statements about the solutions of the Monge and Kantorovich problems, let us introduce some notation from differential geometry. Recall that the *tangent space* (tangent to  $S^{d-1}$ ) at  $\mathbf{x} \in S^{d-1}$  is the  $(d-1)$ -dimensional linear subspace  $\mathcal{T}_{\mathbf{x}}S^{d-1} := \{\mathbf{z} \in \mathbb{R}^d, \mathbf{z}^\top \mathbf{x} = 0\}$ . Letting  $\mathbf{x} \in S^{d-1}$  and  $\mathbf{v} \in \mathcal{T}_{\mathbf{x}}S^{d-1}$ , the directional derivative at  $\mathbf{x} \in S^{d-1}$  of a smooth function  $\zeta: S^{d-1} \rightarrow \mathbb{R}$  in direction  $\mathbf{v}$  is defined as  $v(\zeta) := (\zeta \circ v)'(0)$ , where  $v: [0, 1] \rightarrow S^{d-1}$  is a differentiable path such that  $v(0) = \mathbf{x}$  and  $v'(0) = \mathbf{v}$ . The gradient  $\nabla_{\zeta}(\mathbf{x})$  of  $\zeta$  at  $\mathbf{x} \in S^{d-1}$  then is defined as the vector in  $\mathcal{T}_{\mathbf{x}}S^{d-1}$  such that  $\mathbf{v}^\top \nabla_{\zeta}(\mathbf{x}) = v(\zeta)$  for all  $\mathbf{v} \in \mathcal{T}_{\mathbf{x}}S^{d-1}$  and  $\mathbf{x} \in S^{d-1}$ . The exponential map at a point  $\mathbf{x} \in S^{d-1}$  is a map from the tangent space  $\mathcal{T}_{\mathbf{x}}S^{d-1}$  to  $S^{d-1}$ . More precisely, denoting by  $v_{\mathbf{x}}(t)$  the

unique geodesic with tangent vector  $\mathbf{v} \in \mathcal{T}_{\mathbf{x}}S^{d-1}$  running through  $\mathbf{x} \in S^{d-1}$  ( $v_{\mathbf{x}}(0) = \mathbf{x}$ ), then  $\exp_{\mathbf{x}}(\mathbf{v}) := v_{\mathbf{x}}(1)$ . Finally, consider the following concepts of  $c$ -cyclical monotonicity and  $c$ -convexity.

**Definition 1** A subset  $\Omega \in S^{d-1} \times S^{d-1}$  is called  $c$ -cyclically monotone ( $c$  the squared Riemannian distance on  $S^{d-1}$ ) if, denoting by  $\Sigma(k)$  the set of permutations of  $\{1, \dots, k\}$ , for all  $k \in \mathbb{N}$ , all  $\sigma \in \Sigma(k)$ , and all  $(\mathbf{x}_1, \mathbf{y}_1), \dots, (\mathbf{x}_k, \mathbf{y}_k) \in \Omega$ ,

$$\sum_{i=1}^k c(\mathbf{x}_i, \mathbf{y}_i) \leq \sum_{i=1}^k c(\mathbf{x}_{\sigma(i)}, \mathbf{y}_i).$$

**Definition 2** Two functions  $\psi$  and  $\phi$  from  $S^{d-1}$  to  $\mathbb{R}$  such that

$$\psi(\mathbf{x}) = \sup_{\mathbf{y} \in S^{d-1}} \{\phi(\mathbf{y}) - c(\mathbf{x}, \mathbf{y})\} \text{ and } \phi(\mathbf{y}) = \inf_{\mathbf{x} \in S^{d-1}} \{\psi(\mathbf{x}) + c(\mathbf{x}, \mathbf{y})\} \quad (2.3)$$

are called  $c$ -convex and  $c$ -concave, respectively; call  $\phi$  (resp.  $\psi$ ) the  $c$ -transform of  $\psi$  (resp.  $\phi$ ).

Since the squared Riemannian distance  $c$  satisfies the conditions of Theorem 10.26(i) of Villani (2009), the functions  $\psi$  and  $\phi$  in (2.3) are a.e. differentiable. The following theorem summarizes, for the Monge and Kantorovich problems with transportation cost the squared Riemannian distance on  $S^{d-1}$ , some of the results contained in Chapter 5 of Villani (2009) (for the necessity part of (i), first established by Rüschemdorf (1996)), Theorem 1 of Schachermayer and Teichmann (2008) (for the sufficiency part of (i); see also Pratelli (2008)), Theorems 8 and 9 and Corollary 10 of McCann (2001) (for (ii), (iii), and (iv)). The assumptions made in these references are automatically satisfied here, since  $S^{d-1}$  equipped with the geodesic distance is a Polish metric space and  $c$  is a continuous bounded cost function.

**Proposition 1** Let  $P \in \mathfrak{P}_d$  and  $Q$  denote two probability measures on  $S^{d-1}$ . Then,

- (i) a transport plan  $\gamma \in \Gamma(P, Q)$  is the solution (minimizing  $C_K$  in (2.2) over  $\Gamma(P, Q)$ ) of the Kantorovich problem if and only if it is supported on a  $c$ -cyclically monotone subset of  $S^{d-1} \times S^{d-1}$ ;
- (ii) this solution of the Kantorovich problem exists, is unique, and is of the form  $(I_d \times F)\#P$  where  $F \in S(P, Q)$  is the  $P$ -a.s. unique solution of the corresponding Monge problem (minimizing  $C_M$  in (2.1) over  $S(P, Q)$ );
- (iii) there exist  $c$ -concave differentiable mappings  $\psi$  from  $S^{d-1}$  to  $\mathbb{R}$  such that  $F(\mathbf{x}) = \exp_{\mathbf{x}}(-\nabla\psi(\mathbf{x}))$ ,  $\lambda^{d-1}$ -a.e.

If, moreover,  $Q \in \mathfrak{P}_d$ , then

- (iv)  $\mathbf{Q}(\mathbf{x}) := \exp_{\mathbf{x}}(-\nabla\phi(\mathbf{x}))$ , with  $\phi$  the  $c$ -transform of  $\psi$ , belongs to  $S(Q, P)$ , is the  $Q$ -a.s. unique minimizer of  $C_M$  in (2.1) over  $S(Q, P)$  (i.e., the  $Q$ -a.s. unique solution of the corresponding Monge problem), and satisfies

$$\mathbf{Q}(F(\mathbf{x})) = \mathbf{x} \quad P\text{-a.s.} \quad \text{and} \quad F(\mathbf{Q}(\mathbf{x})) = \mathbf{x} \quad Q\text{-a.s.}$$

Proposition 1 entails the existence of a mapping  $F$  pushing any probability measure  $P \in \mathfrak{P}_d$  forward to any other probability measure  $Q \in \mathfrak{P}_d$  and minimizing, among all such mappings, the transportation cost (2.1). In the next Section, we will use this optimality result to define directional distribution and quantile functions.

Our results all require densities that are bounded away from zero and  $\infty$ . It would be interesting to see if our results and our methods could be extended (i) to densities supported on a subset of the hypersphere and (ii) to other Riemannian manifolds. Encouraging results on the uniform consistency of empirical transports under (i) have been obtained in del Barrio et al. (2020), del Barrio and González-Sanz (2023), and Segers (2023). All these results are limited to the Euclidean case, though, and extending them to the hypersphere is beyond the scope of this paper. As for (ii), whether our methodology adapts to more general Riemannian manifolds, and how, is a challenging question which, definitely, should be left for future research.

### 3 — DIRECTIONAL DISTRIBUTION AND QUANTILE FUNCTIONS

#### 3.1 — Definitions and some basic properties

The concepts of directional distribution and quantile functions we are proposing are based on the optimal transport  $\mathbf{F}$  from a generic probability measure  $\mathbf{P} \in \mathfrak{P}_d$  to the uniform probability measure  $\mathbf{P}^U$  on  $S^{d-1}$ . The idea is inspired by the so-called *center-outward distribution* and *quantile functions*  $\mathbf{F}_\pm$  and  $\mathbf{Q}_\pm := \mathbf{F}_\pm^{-1}$  introduced in Hallin et al. (2021a) for distributions on  $\mathbb{R}^d$ , which involve optimal transports to the spherical uniform over the unit ball. On the hypersphere, the definition of the *directional distribution function* of a random vector  $\mathbf{Z} \sim \mathbf{P}^Z \in \mathfrak{P}_d$  with values on  $S^{d-1}$  is as follows (we indifferently use the expressions *directional distribution and quantile functions of  $\mathbf{Z}$*  and *directional distribution and quantile functions of  $\mathbf{P}^Z$* ).

**Definition 3** Call (directional) distribution function of  $\mathbf{P}^Z \in \mathfrak{P}_d$  the a.s. unique optimal transport map  $\mathbf{F}$  from  $S^{d-1}$  to  $S^{d-1}$  such that  $\mathbf{F}\#\mathbf{P}^Z = \mathbf{P}^U$ .

This definition is very natural, since  $\mathbf{F}$  is such that, for  $\mathbf{Z} \sim \mathbf{P}^Z$ ,  $\mathbf{F}(\mathbf{Z}) \sim \mathbf{P}^U$ —so that  $\mathbf{F}$  has the same probability integral transformation flavor as classical univariate distribution functions. We then have the following important property (see Section ?? of the Supplementary Material for a proof).

**Proposition 2** The distribution function  $\mathbf{F}$  of  $\mathbf{Z} \sim \mathbf{P}^Z \in \mathfrak{P}_d$  is a homeomorphism from  $S^{d-1}$  to  $S^{d-1}$ .

It directly follows from Proposition 2 that the inverse  $\mathbf{Q} := \mathbf{F}^{-1}$  of  $\mathbf{F}$  is well defined, which yields the following definition of a *directional quantile function*.

**Definition 4** Call  $\mathbf{Q} := \mathbf{F}^{-1}$  the directional quantile function of  $\mathbf{P}^Z \in \mathfrak{P}_d$ .

In  $\mathbb{R}^d$ , the *center-outward distribution function*  $\mathbf{F}_\pm$  was defined as an optimal transport to the spherical uniform  $\mathbf{U}_d$  over the unit ball of  $\mathbb{R}^d$ . For  $\mathbf{U}_d$ , nested balls of the form  $\tau S^{d-1}$ , centered at the origin and with  $\mathbf{U}_d$ -probability contents  $\tau$ , naturally play the role of quantile regions of order  $\tau \in [0, 1]$ ; the origin thus naturally qualifies as the median of  $\mathbf{U}_d$ . The center-outward quantile regions then are obtained as the images by  $\mathbf{Q}_\pm := \mathbf{F}_\pm^{-1}$  of these balls.

The basic idea is quite similar in  $S^{d-1}$ . If, however, nested regions with  $\mathbf{P}^U$ -probability contents  $\tau \in [0, 1]$  are to be defined on  $S^{d-1}$ , a central point or *pole*  $\boldsymbol{\theta} \in S^{d-1}$  has to be chosen, playing the role of a directional median for  $\mathbf{P}^Z$ . Since the uniform  $\mathbf{P}^U$  automatically enjoys rotational symmetry with respect to the image  $\mathbf{F}(\boldsymbol{\theta})$  of that pole, the nested regions playing the role of  $\mathbf{P}^U$ -quantile regions should be invariant with respect to rotations with axis  $\mathbf{F}(\boldsymbol{\theta})$ : hence, the collection of spherical caps with  $\mathbf{P}^U$ -probability contents  $\tau$  centered at  $\mathbf{F}(\boldsymbol{\theta})$  naturally qualifies as the family of (nested) quantile regions of orders  $\tau \in [0, 1]$  of  $\mathbf{P}^U$ .

The choice of a directional median or pole  $\boldsymbol{\theta}$ , of course, should be  $\mathbf{P}^Z$ -specific. The literature on directional data provides several concepts of *directional medians*, the most convenient of which is the so-called *Fréchet mean* of  $\mathbf{Z} \sim \mathbf{P}^Z$ , defined as

$$\boldsymbol{\theta}_{\text{Fr}} := \operatorname{argmin}_{\mathbf{z} \in S^{d-1}} \mathbb{E}_{\mathbf{P}^Z} [c(\mathbf{Z}, \mathbf{z})] \quad (3.1)$$

(recall that  $c(\mathbf{z}_1, \mathbf{z}_2)$  denotes the squared Riemannian distance between  $\mathbf{z}_1$  and  $\mathbf{z}_2$ ). The Fréchet mean always exists but is not necessarily unique. In case (3.1) has multiple solutions, one can randomly select  $\boldsymbol{\theta}$  as one of them.

Another possible choice can be based on the transport map  $\mathbf{F}$  (equivalently, on the quantile function  $\mathbf{Q}$ ) itself. For each  $\mathbf{z} \in S^{d-1}$ , consider the hyper-hemisphere  $\mathcal{H}_{\mathbf{z}} := \{\mathbf{u} \in S^{d-1} : \mathbf{u}^\top \mathbf{F}(\mathbf{z}) \geq 0\}$  centered at  $\mathbf{F}(\mathbf{z})$ . Since  $\mathbf{F}$  pushes  $\mathbf{P}^Z$

forward to  $P^U$ , we have that  $P^U(\mathcal{H}_z) = P^Z(Q(\mathcal{H}_z)) = 1/2$ . In general, however,  $Q(\mathcal{H}_z)$  is not a hyper-hemisphere and  $1/2 = P^U(\mathcal{H}_z) \neq P^U(Q(\mathcal{H}_z))$ . A transport-based concept of median for  $P^Z$  is thus

$$\boldsymbol{\theta}_{\text{Tr}} := \operatorname{argmin}_{z \in S^{d-1}} P^U(Q(\mathcal{H}_z)). \quad (3.2)$$

This directional median or pole  $\boldsymbol{\theta}_{\text{Tr}}$  indeed is such that the area of the image by  $Q$  of the hyper-hemisphere centered at  $F(\boldsymbol{\theta}_{\text{Tr}})$  is minimal among the areas of all images  $Q(\mathcal{H}_z)$  of hyper-hemispheres, indicating a concentration of the  $P^Z$  probability mass around  $\boldsymbol{\theta}_{\text{Tr}}$ . Such a pole always exists. Again, it may not be unique and one can randomly select  $\boldsymbol{\theta}$  within the set of points satisfying (3.2).

Assume that a pole  $\boldsymbol{\theta}_M$ , say, has been selected for  $P^Z$  ( $\boldsymbol{\theta}_{\text{Fr}}$  or  $\boldsymbol{\theta}_{\text{Tr}}$  being possible choices). The spherical cap with  $P^U$ -probability  $\tau$  centered at  $F(\boldsymbol{\theta}_M)$  is

$$C_\tau^U := \left\{ \mathbf{u} \in S^{d-1} : F_*(\mathbf{u}^\top F(\boldsymbol{\theta}_M)) \geq 1 - \tau \right\} \quad 0 \leq \tau \leq 1,$$

with boundary

$$C_\tau^U := \left\{ \mathbf{u} \in S^{d-1} : F_*(\mathbf{u}^\top F(\boldsymbol{\theta}_M)) = 1 - \tau \right\} \quad 0 \leq \tau \leq 1, \quad (3.3)$$

(a  $(d-2)$ -sphere) where

$$F_*(u) := \int_{-1}^u (1-s^2)^{(d-3)/2} ds \Big/ \int_{-1}^1 (1-s^2)^{(d-3)/2} ds, \quad -1 \leq u \leq 1. \quad (3.4)$$

Indeed, it is easy to see that  $u \mapsto F_*(u)$  is the distribution function of  $\mathbf{U}^\top F(\boldsymbol{\theta}_M)$  where  $\mathbf{U} \sim P^U$ . Hence,  $F_*(\mathbf{u}^\top F(\boldsymbol{\theta}_M))$  is the  $P^U$ -probability of the  $F(\boldsymbol{\theta}_M)$ -centered spherical cap running through  $\mathbf{u}$  and a measure of  $\mathbf{u}$ 's latitude, ranging from 0 (for  $\mathbf{u} = -F(\boldsymbol{\theta}_M)$ ) to 1 (for  $\mathbf{u} = F(\boldsymbol{\theta}_M)$ ) and scaled in such a way that the latitude of  $\mathbf{U} \sim P^U$  is uniform over  $[0, 1]$ . Therefore, for the hypersphere  $S^{d-1}$  equipped with the uniform distribution  $P^U$  and the pole  $F(\boldsymbol{\theta}_M)$ , the contour  $C_\tau^U$  plays the role of a *parallel* of order  $\tau$  ( $C_{1/2}^U$ , thus, is an *equatorial hypersphere*).

Accordingly, define the quantile contour and quantile region of order  $\tau$  of  $\mathbf{Z} \sim P^Z$  as the images

$$C_\tau := Q\left(C_\tau^U\right) = \left\{ \mathbf{z} \in S^{d-1} : F_*\left(\left(F(\mathbf{z})\right)^\top F(\boldsymbol{\theta}_M)\right) = 1 - \tau \right\} \quad (3.5)$$

and

$$C_\tau := Q\left(C_\tau^U\right) = \left\{ \mathbf{z} \in S^{d-1} : F_*\left(\left(F(\mathbf{z})\right)^\top F(\boldsymbol{\theta}_M)\right) \geq 1 - \tau \right\}, \quad (3.6)$$

by  $Q$  of  $C_\tau^U$  and  $C_\tau^U$ , respectively. Since  $Q$  is a measure-preserving transformation pushing  $P^U$  forward to  $P^Z$ , the  $P^Z$  probability content of  $C_\tau$  is  $\tau$ . The following proposition summarizes the main properties of  $F$ ,  $Q$ , the quantile contours  $C_\tau$  and quantile regions  $C_\tau$ . They all follow from the definitions and the continuity of  $F$  and  $Q$ ; details are left to the reader.

**Proposition 3** Let  $\mathbf{Z} \sim P^Z \in \mathfrak{P}_d$  have distribution and quantile functions  $F$  and  $Q$ , respectively. Then,

- (i)  $F$  entirely characterizes  $P^Z$ ,  $F(\mathbf{Z}) \sim F\#P^Z = P^U$ , and  $F_*\left(\left(F(\mathbf{Z})\right)^\top F(\boldsymbol{\theta}_M)\right) \sim U_{[0,1]}$ ;
- (ii)  $Q$  entirely characterizes  $P^Z$  and  $Q(\mathbf{U}) \sim Q\#P^U = P^Z$ ;
- (iii) the quantile contours  $C_\tau$ ,  $\tau \in [0, 1]$  are continuous; the quantile regions  $C_\tau$  are closed, connected, and nested; their intersection  $\bigcap_{\tau \in [0,1]} C_\tau$  is the directional median  $\boldsymbol{\theta}_M$ ;
- (iv) the probability content  $P^Z(C_\tau)$  of  $C_\tau$ ,  $\tau \in [0, 1]$ , is  $\tau$ , irrespective of  $P^Z \in \mathfrak{P}_d$ .



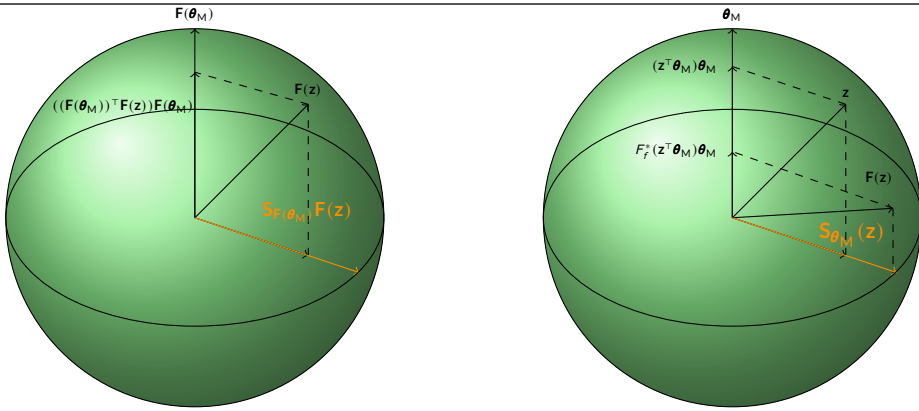


**FIGURE 1** Left: the tangent-normal decomposition of  $\mathbf{F}$  with respect to  $\mathbf{F}(\boldsymbol{\theta}_M)$ . Right: in the rotationally symmetric case, the optimal transport  $\mathbf{F}$  reduces to an optimal univariate transport acting on the projection  $\mathbf{z}^T \boldsymbol{\theta}_M$  of  $\mathbf{z}$  along the rotation axis  $\boldsymbol{\theta}_M$ .

### 3.2 — A natural distribution-specific coordinate system

The quantile function  $\mathbf{Q}$  of  $\mathbf{P}^{\mathbf{Z}}$  actually creates over  $\mathcal{S}^{d-1}$  a coordinate system with latitudes and (hyper)longitudes adapted to the distribution of  $\mathbf{Z}$ .

The usual latitude-(hyper)longitude coordinate system is based on the classical *tangent-normal* decomposition, with respect to a pole  $\mathbf{F}(\boldsymbol{\theta}_M)$ , say, of a point  $\mathbf{u} \in \mathcal{S}^{d-1}$  into the sum of two mutually orthogonal terms

$$\mathbf{u} = (\mathbf{u}^T \mathbf{F}(\boldsymbol{\theta}_M)) \mathbf{F}(\boldsymbol{\theta}_M) + (\mathbf{I}_p - \mathbf{F}(\boldsymbol{\theta}_M) (\mathbf{F}(\boldsymbol{\theta}_M))^T) \mathbf{u} = (\mathbf{u}^T \mathbf{F}(\boldsymbol{\theta}_M)) \mathbf{F}(\boldsymbol{\theta}_M) + \sqrt{1 - (\mathbf{u}^T \mathbf{F}(\boldsymbol{\theta}_M))^2} \mathbf{S}_{\mathbf{F}(\boldsymbol{\theta}_M)}(\mathbf{u}) \quad (3.7)$$

(see the left panel of Figure 1 for  $d = 3$ ) where  $\mathbf{u}^T \mathbf{F}(\boldsymbol{\theta}_M)$ , being constant over the parallel  $\mathcal{C}_\tau^{\mathbf{U}}$  ( $\tau = 1 - F_*(\mathbf{u}^T \mathbf{F}(\boldsymbol{\theta}_M))$ ) defined in Section 3.1, is a latitude while the unit vector (a *directional sign*)

$$\mathbf{S}_{\mathbf{F}(\boldsymbol{\theta}_M)}(\mathbf{u}) := (\mathbf{u} - (\mathbf{u}^T \mathbf{F}(\boldsymbol{\theta}_M)) \mathbf{F}(\boldsymbol{\theta}_M)) / \|\mathbf{u} - (\mathbf{u}^T \mathbf{F}(\boldsymbol{\theta}_M)) \mathbf{F}(\boldsymbol{\theta}_M)\| \quad (3.8)$$

(with the convention  $\mathbf{0}/0 = \mathbf{0}$  for  $\mathbf{u} = \pm \mathbf{F}(\boldsymbol{\theta}_M)$ ) with values on the equatorial hypersphere  $\mathcal{C}_{1/2}^{\mathbf{U}}$ —a hyperlongitude, thus—characterizes hypermeridians  $\mathcal{M}_s^{\mathbf{U}} := \{\mathbf{u} \in \mathcal{S}^{d-1} : \mathbf{S}_{\mathbf{F}(\boldsymbol{\theta}_M)}(\mathbf{u}) = \mathbf{s}\}$ ,  $\mathbf{s} \in \mathcal{C}_{1/2}^{\mathbf{U}}$ .

This parallel/hypermeridian system is well adapted to  $\mathcal{S}^{d-1}$  when equipped with the surface area measure or the uniform measure  $\mathbf{P}^{\mathbf{U}}$ : parallels, for instance, then coincide with  $\mathbf{P}^{\mathbf{U}}$ 's quantile contours  $\mathcal{C}_\tau^{\mathbf{U}}$ , while the hyperlongitudes  $\mathbf{S}_{\mathbf{F}(\boldsymbol{\theta}_M)}(\mathbf{U})$ , for  $\mathbf{U} \sim \mathbf{P}^{\mathbf{U}}$ , are uniform over the equatorial hypersphere. Its image by  $\mathbf{Q}$  is more natural under the probability measure  $\mathbf{P}^{\mathbf{Z}}$ : the same properties, indeed, then hold for the “curvilinear” parallels  $\mathbf{Q}(\mathcal{C}_\tau^{\mathbf{U}}) = \mathcal{C}_\tau$  and the “curvilinear” hypermeridians

$$\mathcal{M}_s := \mathbf{Q}(\mathcal{M}_s^{\mathbf{U}}) := \{\mathbf{z} \in \mathcal{S}^{d-1} : \mathbf{S}_{\mathbf{F}(\boldsymbol{\theta}_M)}(\mathbf{F}(\mathbf{z})) = \mathbf{s}\}, \quad \mathbf{s} \in \mathcal{C}_{1/2}^{\mathbf{U}}. \quad (3.9)$$

### 3.3 — Rotational symmetry

Optimal transports seldom admit closed-form expressions. In the particular case of rotational symmetry, however, explicit expressions for  $\mathbf{F}$  and  $\mathbf{Q}$  are possible.

Consider the rotationally symmetric variable  $\mathbf{Z} \sim \mathbf{P}^{\mathbf{Z}}$  with uniquely defined axis  $\pm\boldsymbol{\theta}$ ; all sensible directional medians  $\boldsymbol{\theta}_{\mathbf{M}}$  (including  $\boldsymbol{\theta}_{\text{Fr}}$  and  $\boldsymbol{\theta}_{\text{Tr}}$ ) then are lying along that axis, and  $\mathbf{P}^{\mathbf{Z}}$  has density (1.2) with  $\boldsymbol{\theta} = \boldsymbol{\theta}_{\mathbf{M}}$ : write  $\mathbf{P}^{\mathbf{Z}} =: \mathbf{P}_{\boldsymbol{\theta}_{\mathbf{M}},f}$ . Denote by

$$F_f(u) := \int_{-1}^u f(s)(1-s^2)^{(\rho-3)/2} ds / \int_{-1}^1 f(s)(1-s^2)^{(\rho-3)/2} ds, \quad -1 \leq u \leq 1,$$

the distribution function of  $\mathbf{Z}^{\top}\boldsymbol{\theta}_{\mathbf{M}}$ , by  $Q_f := F_f^{-1}$  its quantile function. Under rotational symmetry, we have that

$$\mathbf{S}_{\boldsymbol{\theta}_{\mathbf{M}}}(\mathbf{Z}) = (\mathbf{Z} - (\mathbf{Z}^{\top}\boldsymbol{\theta}_{\mathbf{M}})\boldsymbol{\theta}_{\mathbf{M}}) / \|\mathbf{Z} - (\mathbf{Z}^{\top}\boldsymbol{\theta}_{\mathbf{M}})\boldsymbol{\theta}_{\mathbf{M}}\| \quad (3.10)$$

(with the convention that  $\mathbf{0}/0 = \mathbf{0}$ ) is uniformly distributed over the *equatorial hypersphere*

$$\mathcal{S}_{\boldsymbol{\theta}_{\mathbf{M}}}^{d-2} := \left\{ \mathbf{u} \in \mathbb{R}^d : \mathbf{u}^{\top}\boldsymbol{\theta}_{\mathbf{M}} = 0, \mathbf{u}^{\top}\mathbf{u} = 1 \right\} \quad (3.11)$$

(see, e.g., [Paindaveine and Verdebout \(2017\)](#)). Actually,  $\mathbf{S}_{\boldsymbol{\theta}_{\mathbf{M}}}(\mathbf{z})$  is the point in the equatorial sphere with the same *hyperlongitudes* as  $\mathbf{z}$  and can be interpreted as the *directional sign* of  $\mathbf{z}$ . Since  $\mathbf{F}(\mathbf{Z})$ , by definition, is uniformly distributed over  $\mathcal{S}^{d-1}$ ,  $(\mathbf{F}(\mathbf{Z}))^{\top}\boldsymbol{\theta}_{\mathbf{M}}$  has distribution function  $F_*$  as defined in (3.4) and quantile function  $Q_* = F_*^{-1}$ . We then have an explicit form for the directional distribution function  $\mathbf{F}$  of  $\mathbf{Z} \sim \mathbf{P}_{\boldsymbol{\theta}_{\mathbf{M}},f}$  (see Section ?? of the Supplementary Material for a proof).

**Proposition 4** *Let  $\mathbf{Z}$  have rotationally symmetric distribution  $\mathbf{P}_{\boldsymbol{\theta}_{\mathbf{M}},f}$ . Then, letting  $F_f^*(u) := Q_*(F_f(u))$ ,*

$$\mathbf{F}(\mathbf{z}) = F_f^*(\mathbf{z}^{\top}\boldsymbol{\theta}_{\mathbf{M}})\boldsymbol{\theta}_{\mathbf{M}} + \sqrt{1 - (F_f^*(\mathbf{z}^{\top}\boldsymbol{\theta}_{\mathbf{M}}))^2} \mathbf{S}_{\boldsymbol{\theta}_{\mathbf{M}}}(\mathbf{z}). \quad (3.12)$$

Proposition 4 tells us that, in the rotationally symmetric case, the optimal transport  $\mathbf{F}$  essentially reduces to the optimal univariate transport, the function  $F_f^*$  acting on the projection  $\mathbf{z}^{\top}\boldsymbol{\theta}_{\mathbf{M}}$  of  $\mathbf{z}$  onto the axis  $\boldsymbol{\theta}_{\mathbf{M}}$ . This is illustrated in Figure 1 (right panel). A consequence of Proposition 4 is that, in the rotationally symmetric case, our quantile regions coincide with the canonical quantile regions of [Ley et al. \(2014\)](#).

## 4 — EMPIRICAL DISTRIBUTION AND QUANTILE FUNCTIONS, RANKS, AND SIGNS

So far, we have been dealing with population concepts of distribution and quantile functions. If a statistical analysis is to be performed, we need empirical versions of the same; these involve concepts of ranks and signs, which are completely new in the context of directional observations.

### 4.1 — Empirical directional distribution function

Denoting by  $\mathbf{Z}_1^{(n)}, \dots, \mathbf{Z}_n^{(n)}$  a sample of  $n$  i.i.d. observations with distribution  $\mathbf{P}^{\mathbf{Z}}$ , consider a “regular”  $n$ -point grid  $\mathfrak{G}^{(n)} = \{\mathfrak{g}_1^{(n)}, \dots, \mathfrak{g}_n^{(n)}\}$  over the unit hypersphere  $\mathcal{S}^{d-1}$ . In this section, the only property required from  $\mathfrak{G}^{(n)}$

is that the sequence of uniform distributions over the  $n$ -tuple  $\mathfrak{G}_1^{(n)}, \dots, \mathfrak{G}_n^{(n)}$  of gridpoints converges weakly to the uniform distribution  $\mathbb{P}^{\mathbf{U}}$  over  $\mathcal{S}^{d-1}$  as  $n \rightarrow \infty$ .

Since  $\mathbf{F}$  minimizes the transportation cost (2.1), a plugin estimator is obtained as the solution of an optimal coupling problem between the observations and the grid  $\mathfrak{G}^{(n)}$ . More precisely, let  $\mathcal{T}^{(n)}$  denote the set of all permutations of the integers  $\{1, \dots, n\}$ : each permutation  $T \in \mathcal{T}^{(n)}$  defines a bijection  $\mathbf{Z}_i^{(n)} \mapsto \mathfrak{G}_{T(i)}^{(n)}$  between  $\{\mathbf{Z}_1^{(n)}, \dots, \mathbf{Z}_n^{(n)}\}$  and  $\mathfrak{G}^{(n)}$ . The *empirical directional distribution function*  $\mathbf{F}^{(n)}$  is then defined as the mapping

$$\mathbf{F}^{(n)} : \mathbf{Z}^{(n)} := (\mathbf{Z}_1^{(n)}, \dots, \mathbf{Z}_n^{(n)}) \mapsto (\mathbf{F}^{(n)}(\mathbf{Z}_1^{(n)}), \dots, \mathbf{F}^{(n)}(\mathbf{Z}_n^{(n)})) \quad (4.1)$$

satisfying (with  $c(\mathbf{z}_1, \mathbf{z}_2)$  the squared Riemannian distance)

$$\sum_{i=1}^n c(\mathbf{Z}_i^{(n)}, \mathbf{F}^{(n)}(\mathbf{Z}_i^{(n)})) = \min_{T \in \mathcal{T}^{(n)}} \sum_{i=1}^n c(\mathbf{Z}_i^{(n)}, \mathfrak{G}_{T(i)}^{(n)}). \quad (4.2)$$

The terminology *empirical directional distribution function* is justified by the following Glivenko-Cantelli result (see Section ?? of the Supplementary Material for a proof).

**Proposition 5** (Glivenko-Cantelli). *Let  $\mathbf{Z}_1^{(n)}, \dots, \mathbf{Z}_n^{(n)}$  be i.i.d. with distribution  $\mathbb{P}^{\mathbf{Z}}$  over  $\mathcal{S}^{d-1}$ . Then, provided that the sequence of uniform discrete distributions over the  $n$  gridpoints  $\{\mathfrak{G}_1^{(n)}, \dots, \mathfrak{G}_n^{(n)}\}$  of  $\mathfrak{G}^{(n)}$  converges weakly, as  $n \rightarrow \infty$ , to the uniform distribution  $\mathbb{P}^{\mathbf{U}}$  over  $\mathcal{S}^{d-1}$ ,*

$$\max_{1 \leq i \leq n} \|\mathbf{F}^{(n)}(\mathbf{Z}_i^{(n)}) - \mathbf{F}(\mathbf{Z}_i^{(n)})\| \longrightarrow 0 \quad \text{almost surely as } n \rightarrow \infty. \quad (4.3)$$

If a consistent estimation of  $\mathbf{F}$  is the objective, the empirical distribution  $\mathbf{F}^{(n)}$  defined in (4.1), in view of (4.3), offers a perfect solution. If empirical counterparts of the quantile contours and regions  $C_\tau$  and  $\mathcal{C}_\tau$ , hence of the parallels  $C_\tau$  and hypermeridians  $\mathcal{M}_\tau$  (see (3.3) and (3.9)) of Section 3.2 are to be constructed, or if ranks and signs generating a maximal ancillary sigma-field are to be defined, however, more structure is required from the grid  $\mathfrak{G}^{(n)}$ .

## 4.2 — Directional ranks, signs, and empirical quantiles

In this subsection, we show how imposing some additional finite- $n$  structure on the grid  $\mathfrak{G}^{(n)}$  yields empirical versions of  $\mathbf{F}$  with natural data-driven concepts of

- (i) empirical quantile contours and regions consistently estimating the actual ones,
- (ii) a data-driven coordinate system of empirical parallels and hypermeridians adapting to the underlying distribution  $\mathbb{P}^{\mathbf{Z}}$  of the observations, and
- (iii) distribution-free signs and ranks, paving the way to a theory of rank-based inference for directional data with unspecified density.

All these concepts involve a pole  $\boldsymbol{\theta}_M$  (the population Fréchet mean, for instance) or a consistent estimator  $\widehat{\boldsymbol{\theta}}_M^{(n)}$  thereof (e.g., the empirical Fréchet mean). That  $\widehat{\boldsymbol{\theta}}_M^{(n)}$  in turn will define the pole  $\widehat{\boldsymbol{\theta}}^{(n)}$  of a structured grid  $\mathfrak{G}^{(n)}(\widehat{\boldsymbol{\theta}}^{(n)})$  to be used in the estimation of  $\mathbf{F}$ . Accordingly, we are proceeding in two steps: a first step yielding an empirical pole  $\widehat{\boldsymbol{\theta}}^{(n)}$ , then a second step estimating  $\mathbf{F}$  on the basis of the grid  $\mathfrak{G}^{(n)}(\widehat{\boldsymbol{\theta}}^{(n)})$  exploiting the role of  $\widehat{\boldsymbol{\theta}}^{(n)}$  as an empirical pole.

**Step 1.** Construct an empirical version  $\widehat{\boldsymbol{\theta}}^{(n)}$  of the population quantity  $\mathbf{F}(\boldsymbol{\theta}_M)$ . Let  $\widehat{\boldsymbol{\theta}}_M^{(n)}$  be a consistent estimator of  $\boldsymbol{\theta}_M$  and consider an  $n$ -point grid  $\mathfrak{G}_0^{(n)}$  satisfying the assumptions of Proposition 5; denoting by  $\mathbf{F}_0^{(n)}(\mathbf{Z}_i^{(n)})$  the resulting

estimator of  $\mathbf{F}(\mathbf{Z}_i^{(n)})$ , choose  $\widehat{\boldsymbol{\theta}}^{(n)} := \mathbf{F}_0^{(n)}(\mathbf{Z}_i^{(n)})$  where  $\mathbf{Z}_i^{(n)}$  is the sample point closest to  $\widehat{\boldsymbol{\theta}}_M^{(n)}$  in the  $d(\cdot, \cdot)$  metric: Proposition 5 and the continuity of  $\mathbf{F}$  imply that  $\widehat{\boldsymbol{\theta}}^{(n)}$  a.s. converges to  $\mathbf{F}(\boldsymbol{\theta}_M)$ .

**Step 2.** (2a) Construct a further regular grid  $\mathfrak{G}^{(n)}(\widehat{\boldsymbol{\theta}}^{(n)})$  over  $S^{d-1}$ . Factorizing  $n$  into  $n = n_R n_S + n_0$  where  $n_R, n_S, n_0 \in \mathbb{N}$  and  $0 \leq n_0 < \min\{n_R, n_S\}$ , define that grid  $\mathfrak{G}^{(n)}(\widehat{\boldsymbol{\theta}}^{(n)})$  as the product of two independent grids:

- (i) a reference grid  $\mathfrak{E}^{(n_S)} := \{\mathbf{s}_1, \dots, \mathbf{s}_{n_S}\}$  over  $S^{d-2}$ ; again, this grid should be as uniform as possible but the only requirement is the weak convergence, as  $n_S \rightarrow \infty$ , of the uniform distribution over  $\mathfrak{E}^{(n_S)}$  to the uniform over  $S^{d-2}$ . Note that for  $d = 3$ , a fully regular grid  $\mathbf{s}_1, \dots, \mathbf{s}_{n_S}$  is obtained by dividing the unit circle  $S^1$  into  $n_S$  equal parts (see Figure 2);
- (ii) a grid of  $n_R$  points over the unit interval, of the form  $i/(n_R + 1)$ ,  $i = 1, \dots, n_R$ .

(2b) Import the grid  $\mathfrak{E}^{(n_S)}$  of step (2a) to the equatorial space defined by the pole  $\widehat{\boldsymbol{\theta}}^{(n)}$  computed in step 1. More precisely, construct the grid  $\mathfrak{G}^{(n)}(\widehat{\boldsymbol{\theta}}^{(n)})$  that consists in  $n_0$  copies of  $\widehat{\boldsymbol{\theta}}^{(n)}$  (if  $n_0 \neq 0$ ) and the  $n_R n_S$  points  $\mathfrak{G}_{ij}^{(n)}(\widehat{\boldsymbol{\theta}}^{(n)})$  such that

$$1 - F_*((\mathfrak{G}_{ij}^{(n)}(\widehat{\boldsymbol{\theta}}^{(n)}))^\top \widehat{\boldsymbol{\theta}}^{(n)}) = \frac{i}{n_R + 1} \quad \text{and} \quad \mathbf{S}_{\widehat{\boldsymbol{\theta}}^{(n)}}(\mathfrak{G}_{ij}^{(n)}(\widehat{\boldsymbol{\theta}}^{(n)})) = \boldsymbol{\Gamma}_{\widehat{\boldsymbol{\theta}}^{(n)}} \mathbf{s}_j, \quad i = 1, \dots, n_R, j = 1, \dots, n_S$$

where  $\boldsymbol{\Gamma}_\theta$  denotes a  $d \times (d-1)$  semi-orthogonal matrix such that  $\boldsymbol{\Gamma}_\theta \boldsymbol{\Gamma}_\theta^\top = \mathbf{I}_d - \boldsymbol{\theta} \boldsymbol{\theta}^\top$  and  $\boldsymbol{\Gamma}_\theta^\top \boldsymbol{\Gamma}_\theta = \mathbf{I}_{d-1}$ ; the columns of  $(\widehat{\boldsymbol{\theta}}^{(n)}, \boldsymbol{\Gamma}_{\widehat{\boldsymbol{\theta}}^{(n)}})$ , thus, constitute an orthonormal coordinate system of  $\mathbb{R}^d$ , the columns of  $\boldsymbol{\Gamma}_{\widehat{\boldsymbol{\theta}}^{(n)}}$  an arbitrary orthonormal coordinate system of the equatorial hyperplane determined by  $\widehat{\boldsymbol{\theta}}^{(n)}$ . Note that, due to its dependence on  $\widehat{\boldsymbol{\theta}}^{(n)}$ , this grid  $\mathfrak{G}^{(n)}(\widehat{\boldsymbol{\theta}}^{(n)})$  is random.

(2c) Denote by  $\mathbf{F}^{(n)}(\mathbf{Z}_1^{(n)}), \dots, \mathbf{F}^{(n)}(\mathbf{Z}_n^{(n)})$  the solutions of the optimal coupling problem (4.2) based on this second grid  $\mathfrak{G}^{(n)}(\widehat{\boldsymbol{\theta}}^{(n)})$ .

The (directional) empirical sign  $\mathbf{S}_i^{(n)}$  and the (directional) rank  $R_i^{(n)}$  of  $\mathbf{Z}_i^{(n)}$  then are naturally defined as

$$\mathbf{S}_i^{(n)} := \mathbf{S}_{\widehat{\boldsymbol{\theta}}^{(n)}}(\mathbf{F}^{(n)}(\mathbf{Z}_i^{(n)})) \quad (4.4)$$

and

$$R_i^{(n)} = \mathcal{R}^{(n)}(\mathbf{Z}_i^{(n)}) := (n_R + 1) \left[ 1 - F_*((\mathbf{F}^{(n)}(\mathbf{Z}_i^{(n)}))^\top \widehat{\boldsymbol{\theta}}^{(n)}) \right], \quad i = 1, \dots, n \quad (4.5)$$

(with values in  $\{1, \dots, n_R\}$ ), respectively, provided that  $\mathbf{F}^{(n)}(\mathbf{Z}_i^{(n)}) \neq \widehat{\boldsymbol{\theta}}^{(n)}$ ; for  $\mathbf{Z}_i^{(n)}$  such that  $\mathbf{F}^{(n)}(\mathbf{Z}_i^{(n)}) = \widehat{\boldsymbol{\theta}}^{(n)}$ , let  $\mathbf{S}_i^{(n)} := \mathbf{0}$  (the pole has no specific longitude) and  $R_i^{(n)} := 0$ .

The empirical versions of the quantile contours and regions (3.5) and (3.6) are the collections of observations

$$\mathcal{C}_{j/(n_R+1)}^{(n)} := \left\{ \mathbf{Z}_i^{(n)} : R_i^{(n)} = j \right\} \quad \text{and} \quad \mathcal{C}_{j/(n_R+1)}^{(n)} := \left\{ \mathbf{Z}_i^{(n)} : R_i^{(n)} \leq j \right\}, \quad j = 1, \dots, n_R, \quad (4.6)$$

respectively. An empirical quantile contour of order  $j/(n_R + 1)$  (the empirical parallel of order  $j/(n_R + 1)$ ) thus consists of the  $n_S$  sample points with given rank  $j$ . Similarly, the empirical hypermeridian with longitude  $\mathbf{s}$  consists of the  $n_R$  observations with given sign (hyperlongitude)  $\mathbf{s}$ :

$$\mathcal{M}_{\mathbf{s}}^{(n)} := \left\{ \mathbf{Z}_i^{(n)} : \mathbf{F}^{(n)}(\mathbf{Z}_i^{(n)}) \neq \widehat{\boldsymbol{\theta}}^{(n)} \text{ and } \mathbf{S}_i^{(n)} = \mathbf{s} \right\}, \quad \mathbf{s} \in \{ \boldsymbol{\Gamma}_{\widehat{\boldsymbol{\theta}}^{(n)}} \mathbf{s}_1, \dots, \boldsymbol{\Gamma}_{\widehat{\boldsymbol{\theta}}^{(n)}} \mathbf{s}_{n_S} \}. \quad (4.7)$$

Because of the data-driven choice of  $\widehat{\boldsymbol{\theta}}^{(n)}$ , the grid  $\mathfrak{G}^{(n)}(\widehat{\boldsymbol{\theta}}^{(n)})$  is random. If  $n_R \rightarrow \infty$  and  $n_S \rightarrow \infty$ , the assumptions in Proposition 5 are satisfied a.s., and the Glivenko-Cantelli result (4.3) holds a.s. as well. Similar consistency properties then follow for quantile contours and regions, parallels, and hypermeridians. In Supplementary Material A, we establish and discuss several properties—distribution-freeness, ancillarity, and equivariance—of directional signs and ranks.

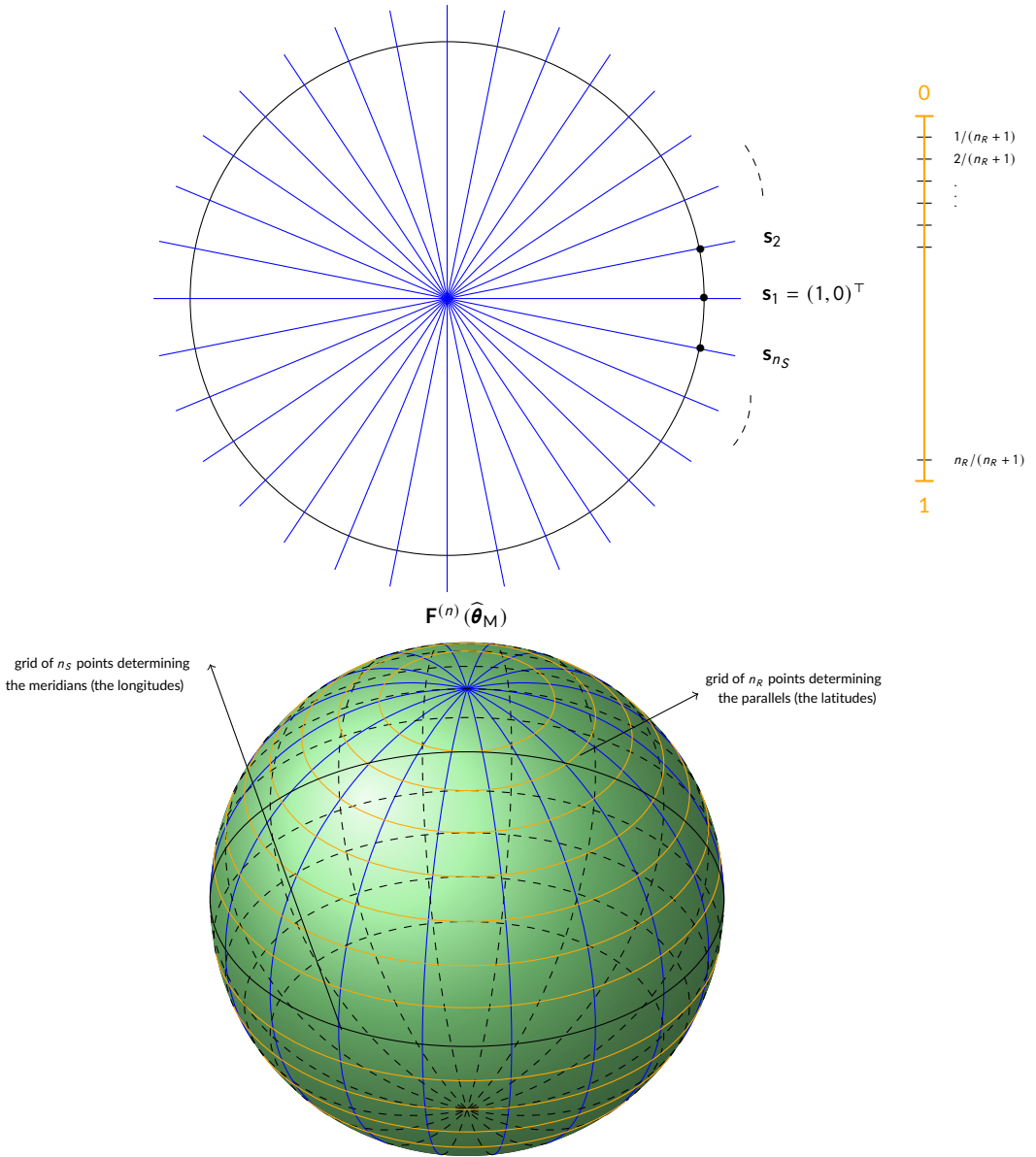


**FIGURE 2** The grid used to define signs and ranks on  $S^{d-1}$  for  $d = 3$ . The final grid is obtained as the product of a reference grid  $\mathfrak{S}^{(n_S)} := \{\mathbf{s}_1, \dots, \mathbf{s}_{n_S}\}$  over  $S^{d-2}$  (here,  $n_S$  equispaced points on the circle  $S^1$ ) and  $n_R$  equispaced points on the unit interval.

### 4.3 — Numerical illustration: simulations

To illustrate the concept of quantile contours in (4.6), we generated sequences of  $n = 2001$  i.i.d. unit random vectors from three types of distributions on  $S^2$ :

- (i) the von Mises–Fisher (vMF) distribution (see (1.1)) with concentration  $\kappa = 10$  and location  $\boldsymbol{\theta} = (0, 0, 1)^\top$ . Below,  $\mathcal{M}_d(\boldsymbol{\theta}, \kappa)$  denotes the von Mises distribution on  $\mathcal{S}^{d-1}$  with location  $\boldsymbol{\theta}$  and concentration  $\kappa$ ;
- (ii) the tangent vMF distribution as defined in García-Portugués et al. (2020). The tangent vMF distribution with location  $\boldsymbol{\theta}$ , angular function  $G$ , skewness direction  $\boldsymbol{\mu}$ , and skewness intensity  $\kappa$  is the distribution of

$$\mathbf{Z} := V\boldsymbol{\theta} + \sqrt{1 - V^2}\boldsymbol{\Gamma}_\boldsymbol{\theta}\mathbf{U}, \quad (4.8)$$

where  $\boldsymbol{\Gamma}_\boldsymbol{\theta}$  is the  $d \times (d - 1)$  semi-orthogonal matrix described in Part (2b) of Step 2 of the construction (Section 4.2) of the grid,  $V$  (an absolutely continuous scalar random variable with values in  $[-1, 1]$ ) and  $\mathbf{U} \sim \mathcal{M}_2(\boldsymbol{\mu}, \kappa)$  are mutually independent; in the simulation, we set  $\boldsymbol{\theta} = (0, 0, 1)^\top$ ,  $\boldsymbol{\mu} = (0.7, \sqrt{0.51})^\top$ ,  $\kappa = 10$ , and  $V = 2\tilde{V} - 1$  with  $\tilde{V} \sim \text{Beta}(2, 8)$ ;

- (iii) a mixture of two vMF distributions—the distribution of  $I[U \leq 0.3]\mathbf{Z}_1 + I[U > 0.3]\mathbf{Z}_2$ , where  $U \sim \text{U}[0, 1]$ ,  $I[\cdot]$  denotes the indicator function, and  $\mathbf{Z}_1 \sim \mathcal{M}_3(\boldsymbol{\theta}_1, \kappa_1)$  and  $\mathbf{Z}_2 \sim \mathcal{M}_3(\boldsymbol{\theta}_2, \kappa_2)$  are mutually independent. In the simulation, we set  $\kappa_1 = 20$ ,  $\boldsymbol{\theta}_1 = (0, -0.5, \sqrt{0.75})^\top$ ,  $\kappa_2 = 20$ , and  $\boldsymbol{\theta}_2 = (0, 0.5, \sqrt{0.75})^\top$ .

For each simulation scheme, we computed the Fréchet mean via the `rbase.robust` function from the R package `RiemBase`. The optimal coupling between the sample points and the regular grid has been obtained by using the fast network simplex algorithm (FNSA) of Bonneel et al. (2011) as implemented in the `transport` function of the R package `transport`. Many efficient algorithms have been proposed for solving the optimal transport problem, e.g., auction algorithm and its refined version (Bertsekas, 1988, 1992). We used the FNSA which is reported in Bonneel et al. (2011) to reduce the complexity of the optimal transport problem from  $O(n^3)$  to  $O(n^2)$ . We factorized  $n$  into  $n_R n_S + n_0$  with  $n_R = 40$ ,  $n_S = 50$  and  $n_0 = 1$ : each empirical quantile contour then consists in 50 points. Plots of the median  $\hat{\boldsymbol{\theta}}^{(n)}$ , the empirical quantile contours for probability contents 12.2% (rank = 5), 48.8% (rank = 20), and 70.7% (rank = 29) are shown in Figures 3 (left, middle, and right panels for the simulation schemes (i), (ii), and (iii), respectively). We also provide in the same figures the corresponding empirical meridians (points with the same signs, same color in the figures).

Under the vMF distribution (Figure 3, left panel), the empirical quantile contours are symmetrically distributed around the median, as expected from the rotational symmetry of the vMF distribution. Under the mixture distribution (Figure 3, middle panel), quantile contours adapt to the underlying multimodality, and the median is located in the mixture component with larger probability weight. Under the tangent vMF distribution, where skewness is involved (Figure 3, right panel), the empirical quantile contours exhibit a distinctive skewed shape. Our empirical quantile contours thus nicely pick up the shapes of the underlying distributions while controlling the probability contents of the corresponding quantile regions.

## 5 — DIRECTIONAL GOODNESS-OF-FIT

Classical goodness-of-fit tests (Kolmogorov–Smirnov, Cramér–von Mises, etc.) are based on distances between distribution functions. Our concepts of population and empirical directional distribution functions quite naturally lead to the construction of directional versions based on distances between  $\mathbf{F}^{(n)}$  and  $\mathbf{F}$ . Assuming that a sample of i.i.d. random unit vectors  $\mathbf{Z}_1^{(n)}, \dots, \mathbf{Z}_n^{(n)}$  have common distribution  $\mathbf{P}^{\mathbf{Z}}$ , the goodness-of-fit problem consists in testing the null hypothesis  $\mathcal{H}_0 : \mathbf{P}^{\mathbf{Z}} = \mathbf{P}_0$  against  $\mathcal{H}_1 : \mathbf{P}^{\mathbf{Z}} \neq \mathbf{P}_0$ , where  $\mathbf{P}_0$  is some specified distribution. This has been studied extensively in directional statistics, with special attention to the problem of testing uniformity—in which case  $\mathbf{P}_0$  is the uniform distribution  $\mathbf{P}^{\mathbf{U}}$  over  $\mathcal{S}^{d-1}$ . In view of Proposition 3, testing  $\mathcal{H}_0 : \mathbf{P}^{\mathbf{Z}} = \mathbf{P}_0$  against  $\mathcal{H}_1 : \mathbf{P}^{\mathbf{Z}} \neq \mathbf{P}_0$  is equivalent to testing  $\mathcal{H}_0 : \mathbf{F} = \mathbf{F}_0$  against  $\mathcal{H}_1 : \mathbf{F} \neq \mathbf{F}_0$  where  $\mathbf{F}_0$  denotes the distribution function of  $\mathbf{P}_0$ —i.e.,  $\mathbf{F}_0(\mathbf{z}) = \mathbf{z}$  in case  $\mathbf{P}_0 = \mathbf{P}^{\mathbf{U}}$ .

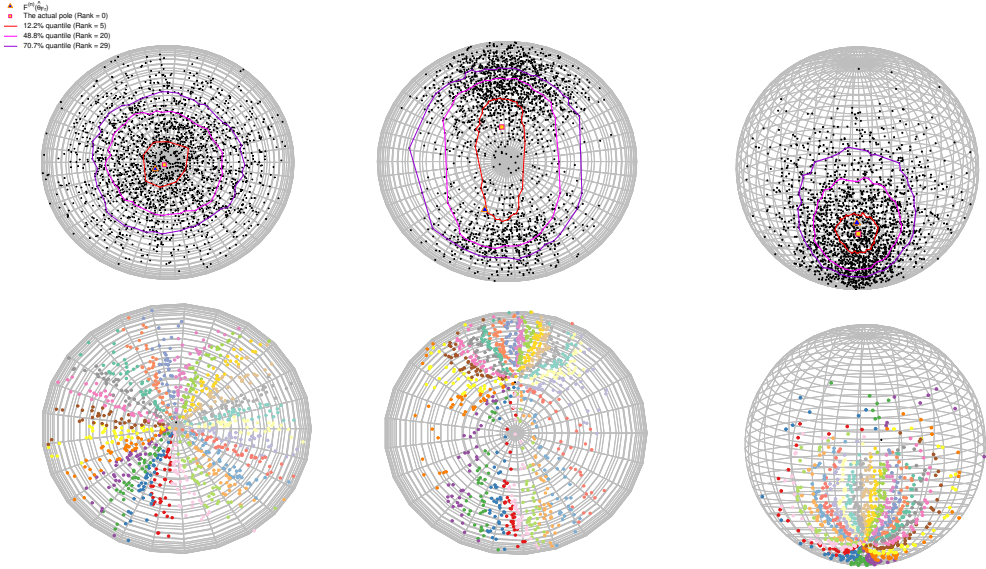


**FIGURE 3** Upper panel: empirical quantile contours (probability contents 12.2%, 48.8%, and 70.7%, respectively) computed from  $n = 2001$  ( $n_R = 40$ ,  $n_S = 50$  and  $n_0 = 1$ ) points drawn from a von Mises-Fisher distribution (left), a mixture of two von Mises-Fisher distributions (middle) and a tangent von Mises-Fisher distribution (right). Lower panel: the corresponding empirical meridians; points with the same color have the same signs.

The test we are proposing in this Section is a Cramér-von Mises-type test that rejects the null hypothesis for large values of the test statistic

$$T_n := n^{-1} \sum_{i=1}^n \left\| \mathbf{F}^{(n)}(\mathbf{Z}_i^{(n)}) - \mathbf{F}_0(\mathbf{Z}_i^{(n)}) \right\|^2, \quad (5.1)$$

where  $\mathbf{F}^{(n)}$  is obtained as in Section 4 (the construction considered in Section 4.1 here is sufficient). That test statistic is the empirical counterpart of the (squared)  $L_2$  distance  $\mathbb{E} \left[ \left\| \mathbf{F}(\mathbf{Z}_i^{(n)}) - \mathbf{F}_0(\mathbf{Z}_i^{(n)}) \right\|^2 \right]$ . As always in goodness-of-fit tests, the critical value  $c_\alpha$  such that  $\mathbb{P}[T_n > c_\alpha] = \alpha$  under  $\mathcal{H}_0$  is easily approximated via Monte Carlo simulations since the null hypothesis is simple; the resulting test thus has exact size  $\alpha$ . The following result establishes its consistency.

**Proposition 6** *Assume that  $\mathbf{Z}_1^{(n)}, \dots, \mathbf{Z}_n^{(n)}$  are i.i.d. with common optimal transport map  $\mathbf{F}$ . Then, provided that the uniform discrete distribution over the  $n$ -points grid  $\mathbb{S}^{(n)}$  converges weakly, as  $n \rightarrow \infty$ , to the uniform distribution  $\mathbf{P}^{\mathbf{U}}$  over  $S^{d-1}$ ,*

- (i)  $T_n = o_{\mathbb{P}}(1)$  as  $n \rightarrow \infty$  under  $\mathcal{H}_0$ , while
- (ii)  $T_n$  converges in probability to a strictly positive constant as  $n \rightarrow \infty$  if  $\mathbf{F} \neq \mathbf{F}_0$ .

It follows from Proposition 6 that the test  $\phi_n$  is asymptotically consistent against any fixed alternative and therefore qualifies as a universally consistent omnibus test.

**Simulations for  $d = 3$ .** In order to investigate the finite-sample performances of our test of uniformity based on (5.1), we performed Monte Carlo size and power comparisons of our test and the projected Cramér-von Mises

(PCvM), projected Anderson-Darling(PAD), and projected Rothman (PRt) tests recently proposed in [García-Portugués et al. \(2023\)](#) and the Rayleigh, Bingham, Ajne, Giné and Bakshaev tests of uniformity ([Rayleigh, 1919](#); [Bingham, 1974](#); [Ajne, 1968](#); [Giné, 1975](#); [Bakshaev, 2010](#)); these tests were implemented in the R package `sphunif`. To do so, we generated  $N = 1000$  independent samples of  $n = 400$  i.i.d. unit random vectors with the following distributions:

- (i) the uniform distribution;
- (ii) vMF distributions, all with location parameter  $\boldsymbol{\theta} = (0, 0, 1)^\top$ , with concentration parameters  $\kappa = 0.05$ ,  $\kappa = 0.1$ , and  $\kappa = 0.5$ ;
- (iii) tangent vMF distributions as in (4.8), all with angular distribution  $F_*$ , location  $\boldsymbol{\theta} = (0, 0, 1)^\top$ , skewness direction  $\boldsymbol{\mu} = (0, 1)^\top$ , and skewness intensities  $\kappa = 0.05$ ,  $\kappa = 0.1$ , and  $\kappa = 0.2$ ;
- (iv) mixtures of two vMFs, of the form  $I[U \leq 0.5]\mathbf{Z}_1 + I[U > 0.5]\mathbf{Z}_2$ , where  $U \sim U[0, 1]$ ,  $\mathbf{Z}_1 \sim \mathcal{M}_3(\boldsymbol{\theta}_1, \kappa_1)$ , and  $\mathbf{Z}_2 \sim \mathcal{M}_3(\boldsymbol{\theta}_2, \kappa_2)$  are mutually independent, with  $\boldsymbol{\theta}_1 = (0, -0.3, \sqrt{0.91})^\top$  and  $\boldsymbol{\theta}_2 = (0.3, \sqrt{0.66}, 0.5)^\top$ , and concentration parameters  $\kappa_1 = \kappa_2 = 0.1$ ,  $\kappa_1 = \kappa_2 = 0.2$ , and  $\kappa_1 = \kappa_2 = 0.3$ ;
- (v) mixtures of two vMFs and a tangent vMF, of the form  $I[U \leq 0.5]\mathbf{Z}_1 + I[0.5 < U < 0.75]\mathbf{Z}_2 + I[U \geq 0.75]\mathbf{Z}_3$ , where  $U \sim U[0, 1]$ ,  $\mathbf{Z}_1$ ,  $\mathbf{Z}_2$  and  $\mathbf{Z}_3$  are mutually independent; with  $\mathbf{Z}_1$  following the tangent vMF distribution as in (iii) with skewness intensities  $\kappa_1 = 0.07$ ,  $\kappa_1 = 0.1$ , and  $\kappa_1 = 0.2$ , and  $\mathbf{Z}_2 \sim \mathcal{M}_p(\boldsymbol{\theta}_2, \kappa_2)$  and  $\mathbf{Z}_3 \sim \mathcal{M}_p(\boldsymbol{\theta}_3, \kappa_3)$  as in scheme (iv) with concentration parameters  $\kappa_2 = \kappa_3 = 0.07$ ,  $\kappa_2 = \kappa_3 = 0.1$ ; and  $\kappa_2 = \kappa_3 = 0.2$ .

In Table 1, we report the rejection frequencies (at nominal level  $\alpha = 0.05$ ), out of  $N = 1000$  replications, of the optimal transport-based Cramér-von Mises test described in (5.1) (OT), the PCvM, PAD, PRt, Rayleigh, Bingham, Ajne, Giné, and Bakshaev tests of uniformity. The critical values are obtained through 2000 Monte Carlo replications. Inspection of Table 1 reveals that all rejection frequencies under the null hypothesis of a uniform distribution are close to the nominal level 0.05. Under the rotationally symmetric vMF alternatives, all tests show similar performances, except for the Bingham and Giné tests, which have significantly lower powers. Under non-rotationally symmetric alternatives such as the tangent vMF or mixture distributions, our test uniformly outperforms all its competitors.

**Simulations for  $d = 2$ .** We investigate, for  $d = 2$ , the finite-sample performance of the same tests by generating  $N = 1000$  replications of  $n = 100$  i.i.d. random vectors from

- (i) the uniform distribution;
- (ii) vMF distributions with location parameter  $\boldsymbol{\theta} = (0, 1)^\top$ , and concentration parameters  $\kappa = 0.05$ ,  $\kappa = 0.1$ , and  $\kappa = 0.5$ ;
- (iii) mixtures of two vMFs, of the form  $I[U \leq 0.7]\mathbf{Z}_1 + I[U > 0.7]\mathbf{Z}_2$ , where  $U \sim U[0, 1]$ ,  $\mathbf{Z}_1 \sim \mathcal{M}_2(\boldsymbol{\theta}_1, \kappa_1)$ , and  $\mathbf{Z}_2 \sim \mathcal{M}_2(\boldsymbol{\theta}_2, \kappa_2)$  are mutually independent, with  $\boldsymbol{\theta}_1 = (-0.3, \sqrt{0.91})^\top$  and  $\boldsymbol{\theta}_2 = (0.6, 0.8)^\top$ , and concentration parameters  $\kappa_1 = \kappa_2 = 0.1$ ,  $\kappa_1 = \kappa_2 = 0.25$ , and  $\kappa_1 = \kappa_2 = 0.5$ ;
- (iv) the sine-skew distribution proposed by [Umbach and Jammalamadaka \(2009\)](#) and [Abe et al. \(2011\)](#), the density of which takes form  $\phi \mapsto f(\phi - \mu)(1 + \lambda \sin(\phi - \mu))$ ,  $\phi \in [-\pi, \pi)$ , where  $f$  is a density (over  $[-\pi, \pi)$ ) symmetric about zero,  $\mu \in [-\pi, \pi)$  is an angular location, and  $\lambda \in (-1, 1)$  a skewness parameter. See [Ley and Verdebout \(2017, Chapter 2\)](#) for the data-generating process. In the simulations, we chose  $f$  to be a vMF density symmetric about 0 with concentration parameters  $\kappa = 0.1$ , set  $\mu = 0$  and  $\lambda = 0.1, 0.3$ , and  $0.35$ .

In Table 2, we report the rejection frequencies (at nominal level  $\alpha = 0.05$ ) of the OT, PCvM, PAD, PRt, Rayleigh, Bingham, Ajne, Giné, and Bakshaev tests of uniformity over  $S^1$ . The results are consistent with those for  $d = 3$  in Table 1. Specifically, all tests have rejection frequencies close to the nominal level under the null hypothesis of uniformity. Under the vMF alternatives, the Bingham and Giné tests have less power than all other ones. Our test outperforms all its competitors whenever skewness or multi-modality are present. Further simulations yielding, in dimension  $d = 5$ , similar conclusions, are provided in the supplementary material.



**TABLE 1** Rejection frequencies of the OT, PCvM, PAD, PRt, Rayleigh, Bingham, Ajne, Giné and Bakshaev tests of uniformity over  $\mathcal{S}^2$  under the uniform, vMF, tangent vMF, mixtures of two vMF distributions and mixtures of two vMFs and a tangent vMF, with various values of concentration or intensity parameter (simulation settings:  $N = 1000$  replications, sample size  $n = 400$ )

|   | OT    | PCvM  | PAD   | PRt   | Rayleigh | Bingham | Ajne  | Giné  | Bakshaev |
|---|-------|-------|-------|-------|----------|---------|-------|-------|----------|
| Uniform   | 0.045 | 0.054 | 0.054 | 0.054 | 0.053    | 0.060   | 0.051 | 0.059 | 0.054    |
| vMF ( $\kappa = 0.05$ )   | 0.078 | 0.076 | 0.073 | 0.072 | 0.070    | 0.052   | 0.072 | 0.053 | 0.076    |
| vMF ( $\kappa = 0.1$ )  | 0.134 | 0.137 | 0.139 | 0.140 | 0.139    | 0.053   | 0.137 | 0.055 | 0.137    |
| vMF ( $\kappa = 0.5$ )  | 0.990 | 0.998 | 0.998 | 0.998 | 0.998    | 0.082   | 0.998 | 0.082 | 0.998    |
| tangent vMF ( $\kappa = 0.05$ )   | 0.073 | 0.042 | 0.042 | 0.044 | 0.050    | 0.031   | 0.051 | 0.03  | 0.042    |
| tangent vMF ( $\kappa = 0.1$ )  | 0.202 | 0.138 | 0.133 | 0.138 | 0.137    | 0.027   | 0.143 | 0.029 | 0.138    |
| tangent vMF ( $\kappa = 0.2$ )  | 0.669 | 0.578 | 0.575 | 0.573 | 0.580    | 0.030   | 0.586 | 0.028 | 0.578    |
| Mixture of two vMFs<br>( $\kappa_1 = \kappa_2 = 0.1$ )                                  | 0.122 | 0.099 | 0.100 | 0.098 | 0.105    | 0.055   | 0.100 | 0.059 | 0.099    |
| Mixture of two vMFs<br>( $\kappa_1 = \kappa_2 = 0.2$ )                                  | 0.325 | 0.303 | 0.302 | 0.297 | 0.295    | 0.058   | 0.297 | 0.061 | 0.303    |
| Mixture of two vMFs<br>( $\kappa_1 = \kappa_2 = 0.3$ )                                  | 0.628 | 0.615 | 0.611 | 0.615 | 0.621    | 0.042   | 0.624 | 0.046 | 0.615    |
| Mixture of two vMFs<br>and a tangent vMF<br>( $\kappa_1 = \kappa_2 = \kappa_3 = 0.07$ ) | 0.117 | 0.108 | 0.112 | 0.108 | 0.102    | 0.074   | 0.104 | 0.077 | 0.108    |
| Mixture of two vMFs<br>and a tangent vMF<br>( $\kappa_1 = \kappa_2 = \kappa_3 = 0.1$ )  | 0.272 | 0.203 | 0.205 | 0.206 | 0.201    | 0.064   | 0.202 | 0.061 | 0.203    |
| Mixture of two vMFs<br>and a tangent vMF<br>( $\kappa_1 = \kappa_2 = \kappa_3 = 0.2$ )  | 0.707 | 0.609 | 0.612 | 0.606 | 0.598    | 0.083   | 0.604 | 0.082 | 0.609    |

## 6 — DIRECTIONAL MANOVA

Let  $\mathbf{X}_{i1}^{(n_i)}, \dots, \mathbf{X}_{in_i}^{(n_i)}, i = 1, \dots, m$ , denote  $m (\geq 2)$  independent samples on the unit hypersphere  $\mathcal{S}^{d-1}$ . For each  $i$ , we assume that  $\mathbf{X}_{i1}^{(n_i)}, \dots, \mathbf{X}_{in_i}^{(n_i)}$  are i.i.d. with common absolutely continuous distribution  $P_i$ , density  $f_i$ , and directional distribution function  $\mathbf{F}_i, i = 1, \dots, m$ . The null hypothesis of interest is the hypothesis  $\mathcal{H}_0 : \mathbf{F}_1 = \dots = \mathbf{F}_m =: \mathbf{F}$  (unspecified  $\mathbf{F}$ ) of no treatment effect.

Let  $\mathbf{F}^{(n)}$  denote the empirical directional distribution function computed from the pooled sample

$$\{\mathbf{Y}_1^{(n)}, \dots, \mathbf{Y}_n^{(n)}\} := \{\mathbf{X}_{11}^{(n_1)}, \dots, \mathbf{X}_{1n_1}^{(n_1)}, \dots, \mathbf{X}_{m1}^{(n_m)}, \dots, \mathbf{X}_{mn_m}^{(n_m)}\}.$$

The tests we propose here are based on a  $(md_J)$ -dimensional statistic  $\Delta_{\mathbf{J}}^{(n)} := ((\Delta_{1;\mathbf{J}}^{(n_1)})^\top, \dots, (\Delta_{m;\mathbf{J}}^{(n_m)})^\top)^\top$  where, for some score function  $\mathbf{J} : \mathcal{S}^{d-1} \rightarrow \mathbb{R}^{d_J}$ ,

**TABLE 2** Rejection frequencies of the OT, PCvM, PAD, PRT, Rayleigh, Bingham, Ajne, Giné, and Bakshaev tests of uniformity over  $S^1$  under the uniform, vMF, mixtures of two vMF distributions and sine-skew distributions (simulation settings:  $N = 1000$  replications, sample size  $n = 100$ )

|   | OT    | PCvM  | PAD   | PRT   | Rayleigh | Bingham | Ajne  | Giné  | Bakshaev |
|---|-------|-------|-------|-------|----------|---------|-------|-------|----------|
| Uniform   | 0.058 | 0.053 | 0.055 | 0.052 | 0.054    | 0.039   | 0.054 | 0.042 | 0.054    |
| vMF ( $\kappa = 0.05$ )                                 | 0.080 | 0.069 | 0.068 | 0.068 | 0.067    | 0.054   | 0.067 | 0.051 | 0.070    |
| vMF ( $\kappa = 0.1$ )                                  | 0.105 | 0.098 | 0.097 | 0.096 | 0.096    | 0.045   | 0.098 | 0.048 | 0.097    |
| vMF ( $\kappa = 0.5$ )                                  | 0.877 | 0.873 | 0.867 | 0.876 | 0.875    | 0.064   | 0.873 | 0.069 | 0.875    |
| Mixture of two vMFs<br>( $\kappa_1 = \kappa_2 = 0.1$ )  | 0.092 | 0.080 | 0.079 | 0.079 | 0.083    | 0.045   | 0.084 | 0.043 | 0.078    |
| Mixture of two vMFs<br>( $\kappa_1 = \kappa_2 = 0.25$ ) | 0.288 | 0.256 | 0.249 | 0.256 | 0.264    | 0.055   | 0.262 | 0.053 | 0.260    |
| Mixture of two vMFs<br>( $\kappa_1 = \kappa_2 = 0.5$ )  | 0.847 | 0.829 | 0.822 | 0.831 | 0.831    | 0.057   | 0.830 | 0.058 | 0.827    |
| Sine-skew ( $\lambda = 0.1$ )                           | 0.093 | 0.080 | 0.079 | 0.084 | 0.081    | 0.041   | 0.081 | 0.041 | 0.080    |
| Sine-skew ( $\lambda = 0.3$ )                           | 0.498 | 0.465 | 0.457 | 0.465 | 0.473    | 0.035   | 0.470 | 0.038 | 0.471    |
| Sine-skew ( $\lambda = 0.35$ )                          | 0.637 | 0.618 | 0.610 | 0.624 | 0.627    | 0.046   | 0.627 | 0.049 | 0.622    |

$$\Delta_{i,j}^{(n_i)} := n_i^{-1/2} \sum_{j=1}^{n_i} \mathbf{J}(\mathbf{F}^{(n)}(\mathbf{X}_{ij}^{(n_i)})) - n^{-1/2} \sum_{\ell=1}^n \frac{n_i^{1/2}}{n^{1/2}} \mathbf{J}(\mathbf{F}^{(n)}(\mathbf{Y}_\ell^{(n)})) = n^{-1/2} \sum_{\ell=1}^n (a_{i\ell}^{(n)} - \bar{a}_i^{(n)}) \mathbf{J}(\mathbf{F}^{(n)}(\mathbf{Y}_\ell^{(n)})), \quad i = 1, \dots, m$$

with  $a_{i\ell}^{(n)} := (n^{1/2}/n_i^{1/2})I[|n_1 + \dots + n_{i-1} + 1 \leq \ell \leq n_1 + \dots + n_{i-1} + n_i]$  and  $\bar{a}_i^{(n)} = n^{-1} \sum_{\ell=1}^n a_{i\ell}^{(n)} = n_i^{1/2}/n^{1/2} (I[\cdot],$  as usual, denotes the indicator function). Below, we assume that  $r_i^{(n)} := n_i/n$  converges to a constant  $0 < r_i < 1$  as  $n \rightarrow \infty$  (possibly, along some subsequence). Letting  $\mathbf{D}_j := \text{Var}(\mathbf{J}(\mathbf{U}))$  where  $\mathbf{U}$  is uniform over  $S^{d-1}$ , our tests reject  $\mathcal{H}_0$  for large values of  $Q_j^{(n)} := (\Delta_j^{(n)})^\top (\mathbf{I}_m \otimes \mathbf{D}_j^-) \Delta_j^{(n)}$ , where  $\mathbf{D}_j^-$  denotes the Moore-Penrose inverse of  $\mathbf{D}_j$ . The next result shows that  $Q_j^{(n)}$  is asymptotically chi-square under  $\mathcal{H}_0$  and some mild regularity assumptions on the score function  $\mathbf{J}$ .

**Proposition 7** Assume that (i)  $\mathbf{J}$  is continuous over  $S^{d-1}$  and (ii)  $\mathbf{J}$  is square-integrable, that is,  $\int_{S^{d-1}} \|\mathbf{J}(\mathbf{u})\|^2 d\mathbf{P}^{\mathbf{U}}(\mathbf{u}) < \infty$ , and (iii) for any sequence  $\mathfrak{G}^{(n)} := \{\mathfrak{G}_1^{(n)}, \dots, \mathfrak{G}_n^{(n)}\}$  of  $n$ -tuples in  $S^{d-1}$  such that the uniform discrete distribution over  $\mathfrak{G}^{(n)}$  converges weakly to  $\mathbf{P}^{\mathbf{U}}$  as  $n \rightarrow \infty$ ,  $\lim_{n \rightarrow \infty} n^{-1} \sum_{\ell=1}^n \|\mathbf{J}(\mathfrak{G}_\ell^{(n)})\|^2 = \int_{S^{d-1}} \|\mathbf{J}(\mathbf{u})\|^2 d\mathbf{P}^{\mathbf{U}}(\mathbf{u})$ . Then, under  $\mathcal{H}_0$  as  $n \rightarrow \infty$ ,  $Q_j^{(n)}$  is asymptotically chi-square with  $(m-1)d^*$  degrees of freedom, where  $d^*$  is the rank of the  $d_j \times d_j$  matrix  $\mathbf{D}_j$ .

The MANOVA tests  $\phi_j^{(n)}$  we are proposing reject the hypothesis of no treatment effect at asymptotic level  $\alpha$  whenever  $Q_j^{(n)} > \chi_{(m-1)d^*, 1-\alpha}^2$  where  $\chi_{p,\tau}^2$  stands for the quantile of order  $\tau$  of a chi-square distribution with  $p$  degrees of freedom. Being based on the  $\mathbf{F}^{(n)}$ -measurable test statistic  $Q_j^{(n)}$ , these tests are fully distribution-free. Below, we investigate their asymptotic properties under local alternatives. To do so, let us consider a parametric framework where the underlying distributions are indexed by some finite-dimensional parameter  $\omega \in \Omega \subset \mathbb{R}^k$ . More precisely, denote by  $\mathbf{P}_{\underline{\omega}}^{(n)}$ , where  $\underline{\omega} := (\omega_1, \dots, \omega_m) \in \Omega^m \subset \mathbb{R}^{mk}$ , the joint distribution of the pooled sample  $(\mathbf{Y}_1^{(n)}, \dots, \mathbf{Y}_n^{(n)})$  when the  $i$ th sample  $(\mathbf{X}_{i1}^{(n_i)}, \dots, \mathbf{X}_{in_i}^{(n_i)})$  has distribution  $\mathbf{P}_{\omega_i}^{(n_i)}$ ,  $i = 1, \dots, m$ . Clearly, under the null hypothesis,  $\mathbf{P}_{\underline{\omega}}^{(n)}$  is of the form  $\mathbf{P}_{(\omega_0, \dots, \omega_0)}^{(n)}$  for some  $\omega_0 \in \Omega$ : write  $\underline{\omega}_0$  for  $(\omega_0, \dots, \omega_0)$ .

In order to study the local power of our tests  $\phi_j^{(n)}$ , consider local alternatives of the form  $\underline{\omega}_0 + n^{-1/2} \boldsymbol{\nu}^{(n)} \boldsymbol{\tau}^{(n)} \in \Omega^m$ , where  $\boldsymbol{\nu}^{(n)} := \text{diag}((r_1^{(n)})^{-1/2} \mathbf{I}_k, \dots, (r_m^{(n)})^{-1/2} \mathbf{I}_k)$  and  $\boldsymbol{\tau}^{(n)} := ((\boldsymbol{\tau}_1^{(n_1)})^\top, \dots, (\boldsymbol{\tau}_m^{(n_m)})^\top)^\top$  with  $\boldsymbol{\tau}_i^{(n_i)}$  a bounded se-

quence of  $\mathbb{R}^k$ . We will assume that the underlying sequence of experiments is sufficiently regular in the sense that, under  $P_{\underline{\omega}_0}^{(n)}$ , as  $n \rightarrow \infty$ ,

$$\Lambda^{(n)} := \log \frac{dP_{\underline{\omega}_0}^{(n)}}{dP_{\underline{\omega}_0}^{(n-1/2, \nu^{(n)} \tau^{(n)})}} = (\boldsymbol{\tau}^{(n)})^\top \boldsymbol{\Delta}_{\underline{\omega}_0}^{(n)} - \frac{1}{2} (\boldsymbol{\tau}^{(n)})^\top \boldsymbol{I}_{\underline{\omega}_0} \boldsymbol{\tau}^{(n)} + o_P(1), \quad (6.1)$$

where  $\boldsymbol{\Delta}_{\underline{\omega}_0}^{(n)} := ((\boldsymbol{\Delta}_{1; \omega_0}^{(n_1)})^\top, \dots, (\boldsymbol{\Delta}_{m; \omega_0}^{(n_m)})^\top)^\top$ , with  $\boldsymbol{\Delta}_{i; \omega_0}^{(n_i)}$  of the form  $\boldsymbol{\Delta}_{i; \omega_0}^{(n_i)} := n_i^{-1/2} \sum_{j=1}^{n_i} \boldsymbol{\varphi}_{\omega_0}(\mathbf{X}_{ij}^{(n_i)})$ ,  $i = 1, \dots, m$  for some square-integrable function  $\boldsymbol{\varphi}_{\omega_0}$ , and  $\boldsymbol{I}_{\underline{\omega}_0} := \text{diag}(\boldsymbol{I}_{1; \omega_0}, \dots, \boldsymbol{I}_{m; \omega_0})$  are such that, still under  $P_{\underline{\omega}_0}^{(n)}$ ,  $\boldsymbol{\Delta}_{\underline{\omega}_0}^{(n)}$  is asymptotically normal with mean  $\mathbf{0}$  and covariance matrix  $\boldsymbol{I}_{\underline{\omega}_0}$ . That is, we assume that the underlying model is LAN with central sequence  $\boldsymbol{\Delta}_{\underline{\omega}_0}^{(n)}$  and information matrix  $\boldsymbol{I}_{\underline{\omega}_0}$ . Letting  $\mathbf{K}_{\mathbf{J}, \omega_0} := \int_{S^{d-1}} \mathbf{J}(\mathbf{u}) \boldsymbol{\varphi}_{\omega_0}(\mathbf{F}^{-1}(\mathbf{u})) dP^{\mathbf{U}}(\mathbf{u})$ , we have the following result.

**Proposition 8** Under  $P_{\underline{\omega}_0}^{(n)}$ ,  $Q_j^{(n)}$  is asymptotically non-central chi-square with  $(m-1)d^*$  degrees of freedom and, letting  $\boldsymbol{\tau}_j := \lim_{n \rightarrow \infty} \boldsymbol{\tau}_j^{(n)}$ , non-centrality parameter  $\sum_{j=1}^m (1-r_j) \boldsymbol{\tau}_j^\top \mathbf{K}_{\mathbf{J}, \omega_0}^\top \mathbf{D}_j^- \mathbf{K}_{\mathbf{J}, \omega_0} \sum_{j=1}^m (1-r_j) \boldsymbol{\tau}_j$ .

Proposition 8 and Le Cam's third lemma readily yield integral expressions (involving the scores  $\mathbf{J}$ , the directional distribution function  $\mathbf{F}^{(n)}$ , and  $\boldsymbol{\varphi}_{\omega_0}$ ) for local and asymptotic powers in this class of parametric models. They also help select a score function  $\mathbf{J}$ : the test based on  $\mathbf{J} = \boldsymbol{\varphi}_{\omega_0} \circ (\mathbf{F}^{(n)})^{-1}$ , for instance, achieves optimality in the parametric LAN model just described. Rather than listing such theoretical expressions for specific LAN models and specific alternatives (location, concentration, multimodality, skewness, ...), we rather provide here a "universal" consistency result for  $\phi_j^{(n)}$ .

**Proposition 9** Let  $\mathbf{X}_{i1}^{(n_i)}, \dots, \mathbf{X}_{in_i}^{(n_i)}$ ,  $i = 1, \dots, m$  be mutually independent samples of i.i.d random directions with directional distribution functions  $\mathbf{F}_i$ ,  $i = 1, \dots, m$  respectively. Assume that there exists a couple  $(i, j)$  such that  $\mathbf{F}_i \neq \mathbf{F}_j$ . Then  $\lim_{n \rightarrow \infty} E[\phi_j^{(n)}] = 1$ .

We conclude this Section by investigating the finite-sample performances of  $\phi_j^{(n)}$  for various scores:

- (i) the uniform score  $\mathbf{J}(\mathbf{u}) := \mathbf{u}$ ;
- (ii) the estimated vMF-location score  $\mathbf{J}(\mathbf{F}^{(n)}(\mathbf{Y}_\ell^{(n)})) := \hat{\kappa} \sqrt{1 - \left(G_{\hat{\kappa}}^{-1} \left(1 - \frac{R_\ell^{(n)}}{n_R + 1}\right)\right)^2} \mathbf{S}_\ell^{(n)}$ , where  $\hat{\kappa}$  is the vMF maximum-likelihood estimator of the concentration parameter,  $G_\kappa$  the distribution function of  $\mathbf{Z}^\top \boldsymbol{\theta}$  with  $\mathbf{Z} \sim \mathcal{M}_d(\boldsymbol{\theta}, \kappa)$ ,  $R_\ell^{(n)} := R^{(n)}(\mathbf{Y}_\ell^{(n)}) = (n_R + 1) \left[1 - F_*((\mathbf{F}^{(n)}(\mathbf{Y}_\ell^{(n)}))^\top \hat{\boldsymbol{\theta}}^{(n)})\right]$ , and  $\mathbf{S}_\ell^{(n)} := \mathbf{S}_{\hat{\boldsymbol{\theta}}^{(n)}}(\mathbf{F}^{(n)}(\mathbf{Y}_\ell^{(n)}))$ ; the estimator  $\hat{\boldsymbol{\theta}}^{(n)}$  is obtained as in Section 4.2, step 1 of the construction of the grid;
- (iii) the estimated vMF-concentration score  $\mathbf{J}(\mathbf{F}^{(n)}(\mathbf{Y}_\ell^{(n)})) := G_{\hat{\kappa}}^{-1} \left(1 - \frac{R_\ell^{(n)}}{n_R + 1}\right)$ , and
- (iv) the estimated vMF-location-concentration score (a linear combination of the scores in (ii) and (iii))

$$\mathbf{J}(\mathbf{F}^{(n)}(\mathbf{Y}_\ell^{(n)})) := \hat{\kappa} \left\{ G_{\hat{\kappa}}^{-1} \left(1 - \frac{R_\ell^{(n)}}{n_R + 1}\right) \hat{\boldsymbol{\theta}}^{(n)} + \sqrt{1 - \left(G_{\hat{\kappa}}^{-1} \left(1 - \frac{R_\ell^{(n)}}{n_R + 1}\right)\right)^2} \mathbf{S}_\ell^{(n)} \right\}.$$

In the simulation exercise below, we compare the resulting tests with their pseudo-vMF (pvMF) counterpart, which rejects the null hypothesis at asymptotic level  $\alpha$  whenever  $Q^{(n)} > \chi_{(m-1)(d-1); 1-\alpha}^2$ , where

$$Q^{(n)} := (d-1) \left( \sum_{i=1}^m \frac{n_i D_i}{E_i} (\bar{\mathbf{X}}_i^{(n_i)})^\top (\mathbf{I}_d - \hat{\boldsymbol{\theta}} \hat{\boldsymbol{\theta}}^\top) \bar{\mathbf{X}}_i^{(n_i)} - \sum_{i,j} \frac{n_i n_j}{n} \frac{D_i D_j}{H} (\bar{\mathbf{X}}_i^{(n_i)})^\top (\mathbf{I}_d - \hat{\boldsymbol{\theta}} \hat{\boldsymbol{\theta}}^\top) \bar{\mathbf{X}}_j^{(n_j)} \right),$$

with  $\hat{\boldsymbol{\theta}}$  the sample Fréchet mean,  $\bar{\mathbf{X}}_i^{(n_i)} := n_i^{-1} \sum_{j=1}^{n_i} \mathbf{X}_{ij}^{(n_i)}$ ,  $E_i := n_i^{-1} \sum_{j=1}^{n_i} (\mathbf{X}_{ij}^{(n_i)})^\top \hat{\boldsymbol{\theta}}$ ,  $H := \sum_{i=1}^m r_i^{(n)} D_i^2 B_i$ ,  $D_i := E_i / B_i$ , and  $B_i := 1 - n_i^{-1} \sum_{j=1}^{n_i} ((\mathbf{X}_{ij}^{(n_i)})^\top \hat{\boldsymbol{\theta}})^2$ ; see Ley et al. (2017) for details.

In the Monte-Carlo simulation, we set  $d = 3$ ,  $m = 2$ ,  $n_1 = 500$ ,  $n_2 = 600$ , hence  $n = 1100$ . The structured regular grid for the computation of the vMF-location, vMF-concentration, and vMF-location-concentration scores was based on  $n_R = 44$ ,  $n_S = 25$ , and  $n_0 = 0$ . The following data-generating processes were considered.

Case (1) (location alternatives):  $\mathbf{X}_{1j}^{(n_1)} \sim \mathcal{M}_d(\boldsymbol{\theta}, \kappa)$ ,  $j = 1, \dots, n_1$  and  $\mathbf{X}_{2\ell}^{(n_2)} \sim \mathcal{M}_d(\mathbf{O}_\xi \boldsymbol{\theta}, \kappa)$ ,  $\ell = 1, \dots, n_2$  where  $\kappa = 3$ ,

$$\boldsymbol{\theta} = \begin{pmatrix} 1 \\ 0 \\ 0 \end{pmatrix}, \quad \text{and} \quad \mathbf{O}_\xi = \begin{pmatrix} \cos(\pi\xi/15) & -\sin(\pi\xi/15) & 0 \\ \sin(\pi\xi/15) & \cos(\pi\xi/15) & 0 \\ 0 & 0 & 1 \end{pmatrix} \quad \text{with } \xi = 0, 0.2, 0.4, 0.6, 0.8; \quad (6.2)$$

Case (2) (concentration alternatives):  $\mathbf{X}_{1j}^{(n_1)} \sim \mathcal{M}_d(\boldsymbol{\theta}, \kappa)$ ,  $j = 1, \dots, n_1$  and  $\mathbf{X}_{2\ell}^{(n_2)} \sim \mathcal{M}_d(\boldsymbol{\theta}, \xi + \kappa)$ ,  $\ell = 1, \dots, n_2$  where  $\kappa = 3$  and  $\boldsymbol{\theta} = (1, 0, 0)^\top$ , with  $\xi = 0, 0.5, 1, 1.5, 2$ ;

Case (3) (multimodal alternatives):  $\mathbf{X}_{1j}^{(n_1)}$ ,  $j = 1, \dots, n_1$ , is a mixture, with mixing probabilities  $\frac{3}{8}$ ,  $\frac{3}{8}$ , and  $\frac{1}{4}$ , of  $\mathcal{M}_d(\boldsymbol{\theta}_1, \kappa_1)$ ,  $\mathcal{M}_d(\boldsymbol{\theta}_2, \kappa_2)$ , and  $\mathcal{M}_d(\boldsymbol{\theta}_3, \kappa_3)$ , where  $\boldsymbol{\theta}_1 = (1, 0, 0)^\top$ ,  $\kappa_1 = 3$ ,  $\boldsymbol{\theta}_2 = (-0.8, 0.3, \sqrt{0.27})^\top$ ,  $\kappa_2 = 2$ ,  $\boldsymbol{\theta}_3 = (0, -0.7, \sqrt{0.51})^\top$ ,  $\kappa_3 = 3$ , and  $\mathbf{X}_{2\ell}^{(n_2)} = \mathbf{O}_\xi \mathbf{Z}_\ell^{(n_2)}$ ,  $\ell = 1, \dots, n_2$ , where  $\mathbf{Z}_\ell^{(n_2)}$  has the same distribution as  $\mathbf{X}_{1j}^{(n_1)}$  and  $\mathbf{O}_\xi$  is as in (6.2) with  $\xi = 0, 1, \dots, 5$ ;

Case (4) (skewed alternatives):  $\mathbf{X}_{1j}^{(n_1)}$ ,  $j = 1, \dots, n_1$  and  $\mathbf{X}_{2\ell}^{(n_2)}$ ,  $\ell = 1, \dots, n_2$  are generated from a tangent vMF dis-

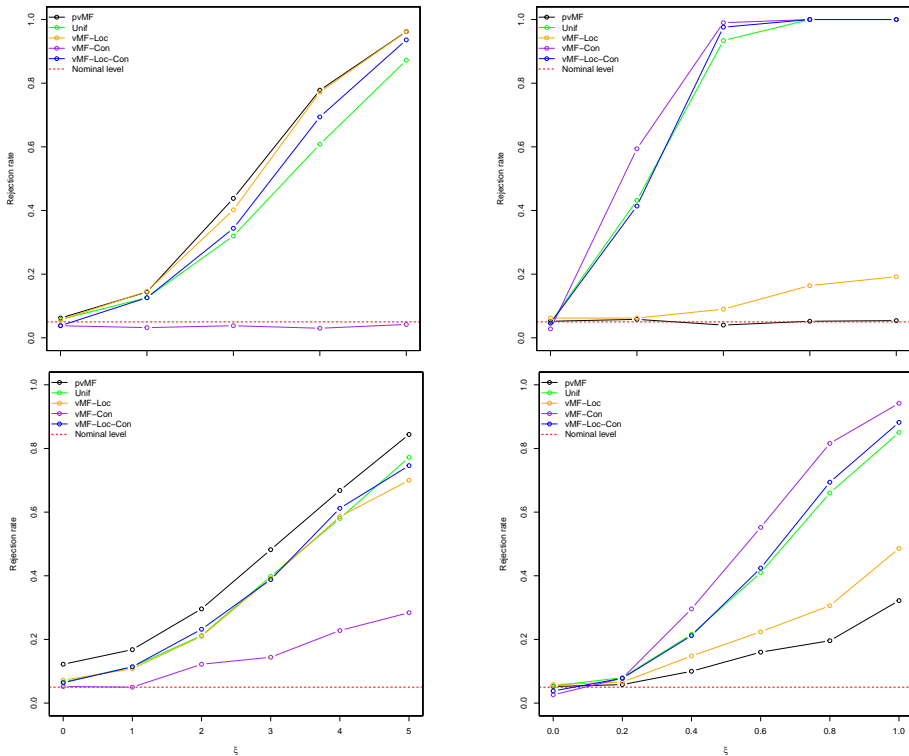


**FIGURE 4** Rejection rates (at 0.05 nominal level) of the pseudo-vMF and rank-based tests with uniform, vMF-location, vMF-concentration, and vMF-location-concentration scores, for Cases (1) (top-left panel), (2) (top-right panel), (3) (bottom-left panel), and (4) (bottom-right panel).

tribution of the form (4.8) with  $\theta = (0, 0, 1)^\top$ ,  $\mu = (0.7, \sqrt{0.51})^\top$ ,  $\kappa = 1$ , with  $\tilde{V} \sim \text{Beta}(2, 5)$  for  $\mathbf{X}_{1j}^{(n_1)}$  and  $\tilde{V} \sim \text{Beta}(2, 5 + \xi)$ ,  $\xi = 0, 0.2, \dots, 1$  for  $\mathbf{X}_{2\ell}^{(n_2)}$ .

For each case, the experiments were repeated 500 times for the directional rank-based tests and the pvMF test at 0.05 nominal level, for the various values of  $\xi$  (where  $\xi = 0$  yields  $\mathcal{H}_0$ ). Figure 4 shows a plot of the rejection frequencies of these tests against  $\xi$ , for Cases (1)–(4). Under the null ( $\xi = 0$ ), all directional rank-based tests yield rejection rates close to the nominal level while the pvMF test exhibits a severe over-rejection frequency of 0.122 under Case (3), revealing a poor behavior under multi-modality. In terms of power, for the vMF location problem (Case (1)), the vMF-location score, uniform score and vMF-location-concentration score rank-based tests all have rejection rates very close to the pvMF test which is the optimal test in this case. For the vMF-concentration parameter problem (Case (2)), the pvMF test has no power and is outperformed by all the directional rank-based tests, the power of which increases with  $\xi$ . For the mixture of three vMF distributions (Case (3)), the rejection frequencies of the pvMF test under the alternative are meaningless in view of its size problem; the uniform, vMF-location, and vMF-location-concentration score rank-based tests have greater power than the vMF-concentration score one. When skewness is present (Case (4)), all the rank-based tests outperform the classical pvMF test. In general, the superiority of the vMF-location-concentration score and uniform score rank-based tests is clear, considering their consistency, sizeable power against multi-modal alternatives, skewness and vMF distributions (both for location and concentration treatment effects). Due to its simplicity, the uniform score is a good choice in terms of computational efficiency.

## 7 – APPLICATION: MANOVA FOR SUNSPOTS DATA

Sunspots are regions on the Sun’s photosphere that are darker and cooler than the surrounding areas. They are caused by concentrations of magnetic flux that inhibit convection and are temporary phenomena that experience continuous changes, lasting for hours to days. Their population first increases rapidly and then decreases slowly over a period of approximately 11 years, which is referred to as the *solar cycle*. Early in a solar cycle, sunspots appear at higher latitudes and then move towards the equator as the cycle approaches maximum, a phenomenon known as *Spörer’s law*. Sunspots are widely used to study and measure solar activity, whose effects may affect earth’s long-term climate (Haigh, 2007).

The data we analyze is based on the Debrecen Photoheliographic Data (DPD) sunspot catalogue, which contains locations of sunspots since 1974 and is a continuation of the Greenwich Photoheliographic Results (GPR) catalogue (spanning 1874-1976). The data is available from the R package `rotasym`.

The sunspots of the 22nd (September 1986 to July 1996;  $n_1 = 4551$  points, in red) and 23rd (August 1996 to November 2008;  $n_2 = 5373$  points, in green) solar cycles are shown in in Figure 5. Visual inspection hardly helps decide whether these two samples are from the same distribution or not. According to García-Portugués et al. (2020), various tests suggest rotational symmetry around the north pole for the 23rd cycle while the same hypothesis is to be rejected ( $p$ -values smaller than 0.02) for the 22nd cycle.

We performed the pvMF and the directional rank-based tests based on the uniform, vMF-location and vMF-concentration scores described in Section 6 for the null hypothesis of equal distributions in the two samples. For the vMF-location and vMF-concentration scores, we factorize  $n = 9924$  into  $n_S = 121$ ,  $n_R = 82$ , and  $n_0 = 2$ . The  $p$ -values of these tests are shown in Table 3. The pvMF test, with  $p$ -value 0.14, does not reject the null of the equality of distributions, even at significance level 0.10. The rank-based test with vMF-concentration scores rejects the same hypothesis at level 0.10, but not at level 0.05. The rank-based tests with uniform, vMF-location and vMF-location-concentration scores, with  $p$ -values at most 0.036, all suggest that the two samples have different distributions. This result is in line

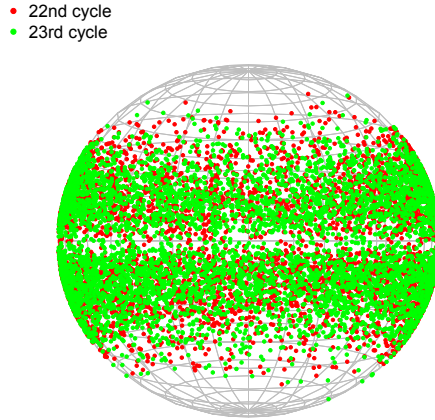


**FIGURE 5** Sunspots data: plot of the sunspots of the 22nd solar cycle ( $n_1 = 4551$  red points) and the 23rd ( $n_2 = 5373$  green points) solar cycle.

| scores      | pvMF  | Unif  | vMF-location | vMF-concentration | vMF-location-concentration |
|-------------|-------|-------|--------------|-------------------|----------------------------|
| $p$ -values | 0.140 | 0.036 | 0.005        | 0.052             | 0.005                      |

**TABLE 3** Sunspots data:  $p$ -values of the pvMF and directional rank-based tests of the equality of distributions of the sunspots of the 22nd and 23rd solar cycles.

with the Monte Carlo experiments (see, e.g., Case (4)), where the directional rank-based tests significantly outperform the pvMF test when the underlying distribution are not rotationally symmetric.

## 8 — CONCLUSIONS

In the present paper, we propose various nonparametric tools, based on optimal transport maps from the underlying distribution to the uniform distribution over the hypersphere, for the analysis of directional data. More precisely, (i) we propose concepts of directional distribution and quantile functions, distribution-free directional signs and ranks, (ii) based on empirical distribution functions, we construct a distribution-free and universally consistent Cramér-von Mises-type test of uniformity on  $S^{d-1}$ , and (iii) based on directional ranks and signs, we develop a class of fully distribution-free MANOVA procedures. Contrary to the pseudo-von Mises methods proposed in the literature—the (asymptotic) validity of which is restricted to rotationally symmetric distributions—our procedures are unrestrictedly finite-sample valid, while outperforming their competitors (particularly so in the absence of rotational symmetry.)

## Acknowledgements

The authors express their warm thanks to Alberto González-Sanz for insightful comments and suggestions on the convergence of empirical transport maps. They also thank the referees and the AE for their their careful reading of the manuscript and their valuable comments that helped improve the manuscript.

## Conflict of Interest Statement

None of the authors are aware of any conflict of interest.

## Data availability

The Sunspots data is available from the R package `rotasym` (García-Portugués et al., 2023).

## references

- Abe, T., Pewsey, A. et al. (2011) Sine-skewed circular distributions. *Statist. Papers*, **52**, 683–707.
- Ajne, B. (1968) A simple test for uniformity of a circular distribution. *Biometrika*, **55**, 343–354.
- Ambrosio, L. and Pratelli, A. (2003) *Existence and Stability Results in the  $L_1$  Theory of Optimal Transportation*, vol. 1813 of *CIME Course, Lecture Notes in Mathematics*. Springer-Verlag Berlin Heidelberg.
- Ameijeiras-Alonso, J., Crujeiras, R. M. and Rodríguez-Casal, A. (2018) Directional statistics for wildfires. In *Applied Directional Statistics* (eds. C. Ley and T. Verdebout), Chapman & Hall/CRC Interdisciplinary Statistics Series, 187–210. Boca Raton: CRC Press.
- Bakshaev, A. (2010)  $N$ -distance tests of uniformity on the hypersphere. *Nonlinear Anal. Model. Control*, **15**, 15–28.
- del Barrio, E. and González-Sanz, A. (2023) Regularity of center-outward distribution functions in non-convex domains. *arXiv:2303.16862*.
- del Barrio, E., González-Sanz, A. and Hallin, M. (2020) A note on the regularity of optimal-transport-based center-outward distribution and quantile functions. *J. Multivar. Anal.*, **180**.
- (2022) Nonparametric multiple-output center-outward quantile regression. *arXiv:2204.11756*.
- Bernoulli, D. (1735) Quelle est la cause physique de l'inclinaison des plans des orbites des planètes par rapport au plan de l'équateur de la révolution du soleil autour de son axe ; et d'où vient que les inclinaisons de ces orbites sont différentes en elles. In *Recueil des pièces qui ont remporté le prix de l'Académie Royale des Sciences* (ed. A. R. des Sciences), vol. 3, 93–122. Paris: Académie Royale des Sciences.
- Bertsekas, D. P. (1988) The auction algorithm: A distributed relaxation method for the assignment problem. *Ann. Oper. Res.*, **14**, 105–123.
- (1992) Auction algorithms for network flow problems: A tutorial introduction. *Comput. Optim. Appl.*, **1**, 7–66.
- Bhattacharya, A. and Bhattacharya, R. (2008) Statistics on Riemannian manifolds: asymptotic distributions and curvature. *Proc. Am. Math. Soc.*, **136**, 2959–2967.
- (2012) *Nonparametric Inference on Manifolds, with Applications to Shape Spaces*. Cambridge University Press.
- Bingham, C. (1974) An antipodally symmetric distribution on the sphere. *Ann. Statist.*, **2**, 1201–1225.
- Bonneel, N., Van De Panne, M., Paris, S. and Heidrich, W. (2011) Displacement interpolation using Lagrangian mass transport. In *Proceedings of the 2011 SIGGRAPH Asia conference*, 1–12.
- Cai, T., Fan, J. and Jiang, T. (2013) Distributions of angles in random packing on spheres. *J. Mach. Learn. Res.*, **14**, 1837–1864.
- Cai, T. and Jiang, T. (2012) Phase transition in limiting distributions of coherence of high-dimensional random matrices. *J. Multivar. Anal.*, **107**, 24–39.

- Chernozhukov, V., Galichon, A., Hallin, M. and Henry, M. (2017) Monge-Kantorovich depth, quantiles, ranks and signs. *Ann. Statist.*, **45**, 223–256.
- Chikuse, Y. (2003) *Statistics on Special Manifolds*, vol. 174 of *Lecture Notes in Statistics*. Heidelberg: Springer.
- Christie, D. (2015) Efficient von Mises-Fisher concentration parameter estimation using Taylor series. *J. Stat. Comput. Simul.*, **85**, 3259–3265.
- Cuesta-Albertos, J. A., Cuevas, A. and Fraiman, R. (2009) On projection-based tests for directional and compositional data. *Stat. Comput.*, **19**, 367–380.
- Cutting, C., Paindaveine, D. and Verdebout, T. (2017) Testing uniformity on high-dimensional spheres against monotone rotationally symmetric alternatives. *Ann. Statist.*, **45**, 1024–1058.
- Deb, N., Bhattacharya, B. B. and Sen, B. (2021) Efficiency lower bounds for distribution-free Hotelling-type two-sample tests based on optimal transport. *arXiv:2104.01986v2*.
- Deb, N. and Sen, B. (2023) Multivariate rank-based distribution-free nonparametric testing using measure transportation. *J. Amer. Statist. Assoc.*, 192–207.
- Dortet-Bernadet, J.-L. and Wicker, N. (2008) Model-based clustering on the unit sphere with an illustration using gene expression profiles. *Biostatistics*, **9**, 66–80.
- Dryden, I. L. (2005) Statistical analysis on high-dimensional spheres and shape spaces. *Ann. Stat.*, **33**, 1643–1665.
- Figueiredo, A. (2006) Two-way analysis of variance for data from a concentrated bipolar Watson distribution. *J. Appl. Stat.*, **33**, 575–581.
- García-Portugués, E., Barros, A. M. G., Crujeiras, R. M., González-Manteiga, W. and Pereira, J. (2014) A test for directional-linear independence, with applications to wildfire orientation and size. *Stoch. Environ. Res. Risk Assess.*, **28**, 1261–1275.
- García-Portugués, E., Navarro-Esteban, P. and Cuesta-Albertos, J. A. (2023) On a projection-based class of uniformity tests on the hypersphere. *Bernoulli*, **29**, 181–204.
- García-Portugués, E., Paindaveine, D. and Verdebout, T. (2020) On optimal tests for rotational symmetry against new classes of hyperspherical distributions. *J. Amer. Statist. Assoc.*, **115**, 1873–1887.
- García-Portugués, E., Paindaveine, D. and Verdebout, T. (2023) *rotasym: Tests for Rotational Symmetry on the Hypersphere*. URL: <https://CRAN.R-project.org/package=rotasym>. R package version 1.1.5.
- García-Portugués, E. and Verdebout, T. (2018) A review of uniformity tests on the hypersphere. *arXiv:1804.00286*.
- Ghosal, P. and Sen, B. (2022) Multivariate ranks and quantiles using optimal transport: Consistency, rates and nonparametric testing. *Ann. Statist.*, **50**, 1012 – 1037. URL: <https://doi.org/10.1214/21-AOS2136>.
- Giné, E. (1975) Invariant tests for uniformity on compact Riemannian manifolds based on Sobolev norms. *Ann. Statist.*, **3**, 1243–1266.
- Haigh, J. D. (2007) The Sun and the Earth's climate. *Living Rev. Sol. Phys.*, **4**, 2.
- Hallin, M. (2022) Measure transportation and statistical decision theory. *Annual Rev. Statist. Appl.*, **9**, 401–424. URL: <https://doi.org/10.1146/annurev-statistics-040220-105948>.
- Hallin, M., del Barrio, E., Cuesta-Albertos, J. A. and Matrán, C. (2021a) Center-outward distribution functions, quantiles, ranks, and signs in  $\mathbb{R}^d$ . *Ann. Statist.*, **48**, 1139–1165.
- Hallin, M., Hlubinka, D. and Hudecová, Š. (2023) Fully distribution-free center-outward rank tests for multiple-output regression and MANOVA. *J. Amer. Statist. Assoc.*, **118**, 1923–1939.



- Hallin, M., La Vecchia, D. and Liu, H. (2022a) Center-outward R-estimation for semiparametric VARMA models. *J. Amer. Statist. Assoc.*, **117**, 925–938.
- (2022b) Rank-based testing for semiparametric VAR models: a measure transportation approach. *Bernoulli*, **29**, 229–273.
- Hallin, M., Mordant, G. and Segers, J. (2021b) Multivariate goodness-of-fit tests based on Wasserstein distance. *Electron. J. Statist.*, **15**, 1328–1371. URL: <https://doi.org/10.1214/21-EJS1816>.
- Hamelryck, T., Kent, J. T. and Krogh, A. (2006) Sampling realistic protein conformations using local structural bias. *PLoS Comput. Biol.*, **2**, e131.
- Jupp, P. E. and Kume, A. (2020) Measures of goodness of fit obtained by almost-canonical transformations on Riemannian manifolds. *J. Multivar. Anal.*, **176**, 104579.
- Kanika, Kumar, S. and SenGupta, A. (2015) A unified approach to decision-theoretic properties of the MLEs for the mean directions of several Langevin distributions. *J. Multivar. Anal.*, **133**, 160–172.
- Kent, J. T. (1982) The Fisher-Bingham distribution on the sphere. *J. R. Stat. Soc. Ser. B Methodol.*, **44**, 71–80.
- Kent, J. T., Bhattacharjee, S., Hussein, I. I., Faber, W. R. and Jah, M. (2018) Fisher-Bingham-Kent mixture models for angles-only observation processing. In *2018 Space Flight Mechanics Meeting*. Reston: American Institute of Aeronautics and Astronautics.
- Kim, P. T., Koo, J.-Y. and Pham Ngoc, T. M. (2016) Supersmooth testing on the sphere over analytic classes. *J. Nonparametr. Stat.*, **28**, 84–115.
- Kolouri, S., Park, S. R., Thorpe, M., Slepcev, D. and Rohde, G. K. (2017) Optimal mass transport: Signal processing and machine-learning applications. *IEEE Signal Process. Mag.*, **34**, 43–59.
- Kulkarni, H. V. and SenGupta, A. (2022) An efficient test for homogeneity of mean directions on the hyper-sphere. *Int. Stat. Rev.*, **90**, 41–61.
- Kume, A., Preston, S. P. and Wood, A. T. A. (2013) Saddlepoint approximations for the normalizing constant of Fisher-Bingham distributions on products of spheres and Stiefel manifolds. *Biometrika*, **100**, 971–984.
- Kume, A. and Sei, T. (2018) On the exact maximum likelihood inference of Fisher-Bingham distributions using an adjusted holonomic gradient method. *Stat. Comput.*, **28**, 835–847.
- Lacour, C. and Pham Ngoc, T. M. (2014) Goodness-of-fit test for noisy directional data. *Bernoulli*, **20**, 2131–2168.
- Ley, C., Sabbah, C. and Verdebout, T. (2014) A new concept of quantiles for directional data and the angular Mahalanobis depth. *Electron. J. Stat.*, **8**, 795–816.
- Ley, C., Swan, Y., Thiam, B. and Verdebout, T. (2013) Optimal R-estimation of a spherical location. *Statist. Sinica*, **23**, 305–332.
- Ley, C., Swan, Y. and Verdebout, T. (2017) Efficient ANOVA for directional data. *Ann. Inst. Statist. Math.*, **69**, 39–62.
- Ley, C. and Verdebout, T. (2017) *Modern Directional Statistics*. Chapman & Hall/CRC. Boca Raton: CRC Press.
- Ley, C. and Verdebout, T. (eds.) (2018) *Applied Directional Statistics*. Chapman & Hall/CRC. Boca Raton: CRC Press.
- Mardia, K. V. and Jupp, P. E. (1999) *Directional Statistics*. Wiley Series in Probability and Statistics. Chichester: Wiley.
- Marinucci, D. and Peccati, G. (2011) *Random Fields on the Sphere*. London Mathematical Society Lecture Note Series. Cambridge: Cambridge University Press.
- Marinucci, D., Pietrobon, D., Balbi, A., Baldi, P., Cabella, P., Kerkycharian, G., Natoli, P., Picard, D. and Vittorio, N. (2008) Spherical needlets for cosmic microwave background data analysis. *Mon. Not. R. Astron. Soc.*, **383**, 539–545.

- McCann, R. J. (1995) Existence and uniqueness of monotone measure-preserving maps. *Duke Math. J.*, **80**, 309–323.
- (2001) Polar factorization of maps on Riemannian manifolds. *Geom. Funct. Anal.*, **11**, 589–608.
- Paindaveine, D. and Verdebout, T. (2017) Inference on the mode of weak directional signals: a Le Cam perspective on hypothesis testing near singularities. *Ann. Statist.*, **45**, 800–832.
- (2020a) Detecting the direction of a signal on high-dimensional spheres: Non-null and Le Cam optimality results. *Probab. Theory Relat. Fields*, **176**, 1165–1216.
- (2020b) Inference for spherical location under high concentration. *Ann. Statist.*, **48**, 2982–2998.
- Pratelli, A. (2008) On the sufficiency of  $c$ -cyclical monotonicity for optimality of transport plans. *Mathematische Zeitschrift*, **258**, 677–690.
- Rao, J. and SenGupta, A. (2001) *Topics in Circular Statistics*, vol. 5 of *Series on Multivariate Analysis*. Singapore: World Scientific.
- Rayleigh, L. (1919) On the problem of random vibrations, and of random flights in one, two, or three dimensions. *Philosophical Magazine*, **37**, 321–347.
- Rüschendorf, L. (1996) On  $c$ -optimal random variables. *Statist. Probab. Lett.*, **27**, 267–270.
- Scealy, J. L. and Wood, A. T. A. (2019) Scaled von Mises–Fisher distributions and regression models for paleomagnetic directional data. *J. Amer. Statist. Assoc.*, **114**, 1547–1560.
- Schachermayer, W. and Teichmann, J. (2008) Characterization of optimal transport plans for the Monge–Kantorovich problem. *Proc. Amer. Math. Soc.*, **137**, 519–529.
- Segers, J. (2023) Graphical and uniform consistency of estimated optimal transport plans. *arXiv preprint arXiv:2208.02508*.
- SenGupta, A. and Kulkarni, H. V. (2020) Universal and efficient tests for homogeneity of mean directions of circular populations. *Stat. Sin.*, **30**, 1995–2021.
- Shi, H., Drton, M. and Han, F. (2022a) Distribution-free consistent independence tests via center-outward ranks and signs. *J. Amer. Statist. Assoc.*, **117**, 395–410. URL: <https://doi.org/10.1080/01621459.2020.1782223>.
- Shi, H., Hallin, M., Drton, M. and Han, F. (2022b) On universally consistent and fully distribution-free rank tests of vector independence. *Ann. Statist.*, **50**, 1933–1959.
- Torous, W., Gunsilius, F. and Rigollet, P. (2022) An optimal transport approach to causal inference. *arXiv:2108.05858*.
- Umbach, D. and Jammalamadaka, S. R. (2009) Building asymmetry into circular distributions. *Stat. Probab. Lett.*, **79**, 659–663.
- Verdebout, T. (2017) On the efficiency of some rank-based test for the homogeneity of concentrations. *J. Stat. Plann. Inference*, **191**, 101–109.
- Villani, C. (2009) *Optimal Transport: Old and New*. Berlin: Springer-Verlag.